The effects of surface roughness on fully developed laminar and transitional flow friction factors and heat transfer coefficients in horizontal circular tubes

Marilize Everts*, Pascal Robbertse, Blayne Spitholt
Department of Mechanical and Aeronautical Engineering, University of Pretoria, South Africa

Abstract

Although the effect of surface roughness on internal forced convection is considered a mature field, very limited work has been done focussing on the effect of surface roughness in the laminar and transitional flow regimes, especially for fully developed flow. Therefore, the purpose of this study was to experimentally investigate the simultaneous heat transfer and pressure drop characteristics in the laminar and transitional flow regimes for tubes with internally roughened surfaces. Experiments were performed using circular tubes with an internal diameter of 5.14 mm and a length of 5.45 m, with the smooth tube having a relative surface roughness close to 0, and the rough tubes having relative surface roughness values of 0.0003 and 0.0006. Water was used as the test fluid and the experiments were performed for Reynolds numbers between 500 and 9 800, while the Prandtl number varied between 4.32 and 7.01. Three different constant heat fluxes with values of 1, 2 and 3 kW/m^2 were applied to the test section while determining the friction factors from the pressure drop measurements and the heat transfer coefficients, Nusselt numbers and Colburn *j*-factors, from the measured fluid and surface temperatures. The Colburn *j*-factors and friction factors behaved similarly throughout the tested Reynolds range and the flow regime boundaries of the heat transfer and pressure drop results corresponded well. An increase in surface roughness favoured an increase in heat transfer in the laminar flow regime, but not in the other flow regimes. When investigating the influence of surface roughness on the critical Reynolds number, three distinct regions were identified and defined, namely, the Dampening region, Enhancing region and Saturating region. For low values of relative surface roughness, the onset of transition was delayed, while transition occurred earlier as the relative surface roughness was increased to moderate and high values. General trends in all three regions were that, an increase in surface roughness decreased the width of the transitional flow regime while increasing the transition gradient.

Key words:
surface roughness; heat transfer; pressure drop; transitional flow; horizontal tubes.

* Corresponding author: marilize.everts@up.ac.za (M. Everts).

Nomenclature

A	Surface area
C_p	Specific heat capacity
D	Inner diameter of tube
EB	Energy balance
f	Friction factor
FS	Full scale
g	Gravitational acceleration
Gr	Grashof number
H	Heat transfer coefficient
j	Colburn j-factor
k	Thermal conductivity
L	Length of tube
Lt	Thermal entrance length
$\dot{m}$	Mass flow rate
Nu	Nusselt number
ΔP	Pressure drop
Pr	Prandtl number
$\dot{q}$	Heat flux
$\dot{Q}_w$	Heat transfer rate to water
$\dot{Q}_e$	Electric heat transfer rate
Ra	Rayleigh number
R_a	Arithmetic mean roughness
Re	Reynolds number
R_z	Roughness depth
T	Temperature
$\dot{V}$	Volumetric flow rate
x	Axial position

Greek symbols

β	Volume expansion coefficient
ε	Surface roughness height
ε_{eff}	Effective surface roughness height
Δ	Change in quantity
μ	Dynamic viscosity of fluid
υ	Kinematic viscosity
ρ	Density of fluid

Subscripts

b	Bulk
c	Constricted
cr	critical
e	Exit/Outlet
FC	Forced convection
FD	Fully developed
h	Heated
i	Inlet
m	Mean
o	Outer
qt	Quasi-turbulent
s	Surface
t	Tube/Turbulent
w	Water

Superscripts

*	Modified

1. Introduction

Heat exchangers are essential components in heating and cooling processes that are used in a variety of applications that range from commercial use, such as refrigeration and air conditioning, to industrial processes such as solar, nuclear and fossil fuel power generation and petrochemical plants. In the process of the design and development of heat exchangers, the influence of the surface roughness is an important factor to take into consideration. The surface roughness influences the pressure drop and thus the pumping power, as well as the heat transfer rate and thus the size of the heat exchanger.

Rough tubes can be considered to be in one of two categories: enhanced tubes which typically have two-dimensional periodic roughnesses, and "naturally" rough tubes which typically have three-dimensional random roughnesses. Enhanced tubes are manufactured with periodic surface roughness elements with defined uniform shapes. Although enhanced tube geometries are generally very successful in improving the heat transfer rates in the turbulent [1, 2] and transitional [2-5] flow regimes, it is not very effective in the laminar flow regime [1, 2]. Improvements of the heat transfer in the laminar flow regime are attributed to induced bulk fluid motion, typically flow swirl [1, 6]. Examples of swirl inducing enhanced tubes include helically finned and corrugated tubes [6]. Alternatively, enhanced tubes such as knurled tubes [7], more closely resemble the mechanism of near wall flow disturbances, typical of naturally rough surfaces.

The second category of rough tubes is where the elements of naturally rough tubes are in some manner imitated. The roughness elements of naturally rough surfaces have non-uniform random shapes, sizes, and distributions which can arise from manufacturing processes, corrosion, chemical etching or fouling on the tube surfaces [8]. Sand-grain roughened tubes are different from naturally rough tubes, because the size of the roughness elements in sand-grain roughened tubes are uniform (non-random) [8]. Furthermore, in sand-grain roughened tubes, cavities exist between the grains of sand [9], which are not present in naturally rough tubes. The roughness elements in this study, where the surface roughness was produced using a sand blasting technique, more closely resembles naturally rough surfaces due to the roughness profile consisting of randomly sized peaks and troughs. The category of naturally rough tubes was therefore the focus of this study.

Rough tubes were first investigated in the nineteenth century by Darcy [10] and later Fanning [11] developed a correlation to calculate the friction factors as a function of surface roughness [12]. The pioneering work on quantifying the influence of surface roughness on the friction factors was conducted by Nikuradse [9] in 1932, who measured the pressure drop over six different macro-scale tubes which had been roughened by gluing sand grains of different uniform sizes to the inner surface of tubes. Based on his experimental results, Nikuradse divided the flow regimes of rough tubes into three distinct ranges: (1) the laminar flow regime in which the friction factor decreased with increasing Reynolds number, (2) the transitional flow regime, which started at a Reynolds number of approximately 2 000 and the friction factor increased with increasing Reynolds numbers, and (3) the turbulent flow regime in which the friction factor was approximately independent of Reynolds number. A few years later Colebrook [13] published his findings on the effect of surface roughness on the pressure drop in macro-tubes.

One of the most widely used resources for determining the friction factors over a wide range of Reynolds numbers in rough tubes is the Moody chart [14]. This chart was produced primarily using the data from the extensive experimental work of Nikuradse [9] and is essentially the Colebrook equation [13] plotted over a wide range of Reynolds numbers and

relative surface roughnesses up to 0.05. This early work laid the foundation for the understanding of the effects of the surface roughness on the friction factor in the various flow regimes. It follows from the Moody chart that the laminar friction factors are independent of surface roughness, while an increase in surface roughness leads to an increase in friction factors in the turbulent flow regime. Unfortunately, the Moody chart does not provide information on the influence of surface roughness on the transition from laminar to turbulent flow.

Parameters such as the arithmetic mean roughness height, R_a, and the mean peak-to-peak roughness height, R_z, have generally been used to quantify the mean surface roughness height, ε, of tubes with non-uniform roughnesses. Different roughness parameters produce vastly different results due to the underlying algorithms used to calculate them and it should also be noted that these algorithms do not resemble the method for determining roughness by the diameter of sand-grains. In the experiments of Nikuradse, the mean roughness height, ε, was determined from the mean height (size) of the sand grains. However, it is important to note that after the sand grains were glued to the inside of the tube using Japanese lacquer, the tubes were refilled with lacquer, emptied, and left to dry for approximately 2-3 weeks to improve adherence of the sand grains to the tubes [9]. The thin coat of lacquer which remained on the sand grains reduced the relative surface roughness to range between 0 and 0.033 [15].

Webb *et al*. [16] found that flow that is separated from the surface due to a roughness element, typically reattaches to the surfaces after a distance of 6-8 times the height of the roughness element. This becomes significant at increased values of relative surface roughness, because the flow does not reattach to the tube wall and therefore decreases the available flow area. As the effective diameter of the flow is no longer the inner (or base) diameter of the tube, Kandlikar *et al*. [12] introduced the constricted flow diameter, D_c, to account for the reduced size due to the roughness elements. To obtain the constricted diameter, two times the roughness height (ε) is subtracted from the inner diameter of the tube.

Kandlikar *et al*. [12] therefore developed a modified Moody chart that uses the constricted diameter for the relative surface roughness, Reynolds number and Colebrook equation. Although the modified Moody chart appears to be similar to the original Moody chart, one major difference is that for $\varepsilon/D_c > 0.03$ the turbulent friction factors collapse onto a single line and become independent of surface roughness. The diameter more likely to be employed by engineers would be based on a practical measurement of the inner tube diameter, which better corresponds to the constricted diameter, while the Moody chart was developed using the base diameter of the tube, before grains of sand were glued to its surface.

This explains why when the mean height of the surface roughness was determined by direct profile measurements, the friction factors do not necessarily correspond to those in the Moody chart. It is for this reason that the concept of effective surface roughness, $\varepsilon_{eff,}$ or the effective relative surface roughness, ε_{eff}/D, is used in literature [8, 15, 17-21]. Effective surface roughness represents the roughness that is back-calculated from experimental friction factor results rather than using the physical measurement of the surface roughness profile. In other words, the effective surface roughness is the roughness that is expected to be achieved from the Moody chart when a specific friction factor is determined from pressure drop measurements.

Any irregularities or roughness on the tube surface can lead to disturbances in the laminar sublayers near the tube surface. In the laminar flow regime, where the fluid flows in parallel streamlined layers that slide over one another, the disturbances caused by rough surfaces affect the fluid layers closest to the tube surface causing them to become curved [22], while the flow in the centre of the tube remains parallel and unchanged. In conventional laminar theory for

macro-scale tubes, the hydrodynamic and thermal boundary layers are not significantly changed, therefore, the surface roughness was found to have little effect on the friction factors and heat transfer coefficients in the laminar flow regime [1, 9, 14, 23]. This is because the proportion of disturbed flow in the tube is small compared to the parallel flow. However, Huang *et al*. [22] found that surface roughness started affecting the laminar friction factors in macro-tubes when the relative surface roughness exceeded 0.07.

In micro-tubes, the relative surface roughness values are significantly higher than for macro-tubes, due to the small tube diameters. Due to the wide range of applications of mini- and micro-tube heat exchangers, several studies focused on the effect of surface roughness on the laminar friction factors in these small diameter tubes. Previous studies focussing on micro-tubes found that, contrary to conventional laminar theory, an increase in surface roughness led to an increase in the laminar friction factors [12, 15, 19, 20, 24]. The cause of this increase in friction factors was attributed to the increase in surface roughness [21]. When plotting the friction factors in terms of the constricted flow diameter, it was found that the laminar friction factors indeed correlated well with conventional laminar theory [12, 15, 20-22, 25, 26]. However, Ghajar *et al*. [21] pointed out that when plotting the results in terms of the constricted flow parameters, the surface roughness is actually disregarded, as it only considers the free flow area that corresponds to the constricted flow diameter.

Kandlikar [15] suggested that it is possible that roughness effects in the laminar flow regime were limited to micro- and mini-scale tubes, however, after reviewing the experimental work of Nikuradse [9], he proposed that high uncertainties in the experimental work could have led to improperly concluding that there were no roughness effects in the laminar flow regime for relative surface roughnesses below 0.05. It was recommended that experiments investigating the effects of the surface roughness in the laminar flow regime for macro-scale tubes (> 3 mm) should be done to confirm this proposition.

Unlike the laminar flow regime, the friction factors and heat transfer coefficients in the transitional and turbulent flow regimes are strong functions of surface roughness [21, 23]. In the transitional and turbulent flow regimes, the viscous boundary layers, where the majority of the temperature and velocity gradients occur, are thin and close to the wall. Therefore, by disturbing this boundary layer, the pressure drop and heat transfer characteristics are affected.

Several studies have been conducted to investigate the effect of surface roughness on friction factors in the transitional flow regime using micro- and mini-tubes, as well as micro- and mini-channels. A common finding in these studies is that the start of the transitional flow regime occurred at lower Reynolds numbers for an increase in surface roughness [15, 19-21, 25, 27, 28]. Based on the constricted flow diameter, correlations were developed to predict the critical Reynolds number in rectangular mini-channels for $0 < \varepsilon/D_{h,cf} \leq 0.08$ and $0.08 < \varepsilon/D_{h,cf} \leq 0.15$ for isothermal conditions [12, 25]. An interesting observation made by Tam *et al*. [28] and Ghajar *et al.* [21] was that in the larger tubes (> 0.838 mm), the surface roughness showed no influence on transition, and for the smaller tubes (≤ 0.838 mm), the increase in the relative surface roughness advanced the onset of transition. Ghajar *et al.* [21] noted that for small diameters (micro-channels), the tolerances and non-uniformity of the tube diameter can lead to significantly higher effective surface roughness, ε_{eff}, than the measured mean roughness, R_a. This could be a partial explanation for the difference observed in the behaviour between mini- and micro-channels that have similar relative surface roughnesses determined by R_a.

Previous studies [15, 19-21, 25, 27] considered only the isothermal friction factors, while Tam *et al*. [28] considered both isothermal and diabatic friction factors. Tam *et al*. [28] found that heating delayed the onset of transition for rough tubes, but had a negligible effect on the

end of transition. Similar findings were obtained by Everts and Meyer [29] when investigating smooth tubes.

As the influence of surface roughness had a greater effect on the start of the transitional flow regime, than the end of the transitional flow regime, it also affected the width of the transitional flow regime, which represents the Reynolds number range in which transition occurs [29]. However, except for Tam *et al*. [28], previous studies in micro- and mini-tubes only focussed on the effect of surface roughness on the critical Reynolds number and not on the end and width of the transitional flow regime. The authors found that the width of the transitional flow regime decreased with increasing surface roughness.

The start of the transitional flow regime, is usually considered to correspond to the Reynolds number at which the gradient of the friction factors of Colburn-*j* factors changes from negative to positive, therefore the 'trough' in the friction factor or Colburn-*j* factor results [29, 30]. However, Ghajar *et al*. [21] and Tam *et al*. [28] considered the start of the transitional flow regime to correspond to the Reynolds number at which the friction factors started to deviate more than 5% from the conventional laminar theory ($f = 64/Re$). This Reynolds number might not necessarily represent the critical Reynolds number, as previous studies conducted by Idelchick [31], Celata *et al*. [32] and Zhao and Liu [33] also found that the laminar friction factors began to deviate from theory at Reynolds numbers of 585 and 800, respectively. Idelchick [31] proposed a correlation to predict this Reynolds number that corresponds to the deviation from the conventional laminar theory. This increase in the friction factor (deviation) was due to the surface roughness which caused an increase in flow resistance by breaking up the laminar boundary layer [31]. If this point is considered to be the critical Reynolds number, the width of the transitional flow regime will appear significantly wider than what it should be and the gradient of the transitional flow regime will be miscalculated.

To the authors' best knowledge, only two studies [22, 26] investigated the effect of surface roughness on friction factors in the transitional flow regime using macro-tubes. A significant relative surface roughness can be obtained in mini- and micro-tubes using methods such as acid etching [15, 19, 20, 28], sanding [20] or by considering the surface finish of the tube itself when the diameters are very small [21]. That is, a smooth micro-tube may have the same relative surface roughness value as a rough macro-tube. The limited studies conducted to date using macro-tubes might be due to the difficulty in obtaining a significant relative surface roughness in larger diameter tubes. Similar to Nikuradse [9], Huang *et al.* [22, 26] roughened their tubes by gluing sand grains of different sizes to the inside. It was found that an increase in surface roughness decreased the critical Reynolds number, as well as the width of the transitional flow regime. These studies focused on isothermal friction factors only, and no heating was applied.

While Nikuradse [9] probably conducted the most complete study investigating the effect of surface roughness on friction factors, Dipprey and Sabersky [8] noted that the effect of surface roughness on heat transfer coefficients received much less attention, especially for sand-grain roughened tubes. This is most probably due to the fact that a complete study would require very accurate heat transfer measurements and a wide range of Prandtl numbers, where obtaining accurate heat transfer data is challenging due to the thermal resistance that the sand and glue imparted on the tubes [34, 35].

Dipprey and Sabersky [8], therefore sought to extend the experimental friction factor work of Nikuradse [9], by conducting a study on the effect of the surface roughness on both the friction factors and the heat transfer coefficients in the turbulent flow regime using water in sand-grain-like roughened tubes. The tubes were manufactured by electroplating nickel over mandrels

coated with sand grains of different sizes. The mandrels and the sand were subsequently chemically dissolved, leaving the nickel tubes with rough surfaces with effective relative surface roughness, ε_{eff}/D, between 0.0024 and 0.049. It was found that heat transfer coefficients increased with the increase in the surface roughness [8]. The heat transfer coefficients and friction factors, however, did not increase proportionally, but generally favoured the increase in the friction factors. An exception to this was in a transition region for tubes with surface roughnesses that varied between smooth and fully rough.

To the authors' best knowledge, the only studies that focussed on the influence of surface roughness on heat transfer in the transitional flow regime, are those conducted by Kandlikar *et al.* [19] and Everts *et al.* [34, 35]. The transitional flow regime is an area of interest, as it provides a good compromise between the low pressure drops and low heat transfer rates in the laminar flow regime, and the high heat transfer rates and high pressure drops in the turbulent flow regime [36]. In this flow regime, tubes with roughened surfaces can be used to further increase the heat transfer coefficients [23, 34-36].

Kandlikar *et al.* [19] investigated heat transfer in stainless-steel mini-tubes with diameters of 1 067 μm and 620 μm, where the internal surfaces were acid etched, resulting in different relative surface roughnesses between 0.001 and 0.003 (based on R_a). In the 1 067μm tube, it was found that the surface roughness had no effect. The smaller 620 μm tube, for the same relative surface roughnesses as those of the larger tube, showed increased Nusselt numbers in the laminar flow regime and the transitional flow regime started at lower Reynolds numbers.

By using adhesive and uniformly sized sand grains to roughen tubes, Everts *et al.* [34, 35] focused specifically on the transitional flow regime, while significant portions of the laminar and turbulent flow regimes were also investigated. This study provided good qualitative heat transfer results that showed the expected trends in the transitional flow regime. It was found that the surface roughness increased the heat transfer coefficients and also advanced the onset of transition. However, this study could only provide qualitative heat transfer results due to the difficulty in characterising the thermal resistance that the adhesive and sand grains imparted on the tube. The experiments were thus not considered quantitatively accurate.

The ranges of the relative surface roughnesses from the relevant previous studies have been summarised in Fig. 1 and are coloured according to the metric that the surface roughness was based on. This figure indicates that the relative surface roughness that was attained in macro-tubes in the present study, are an order of magnitude lower than that attained in mini-tubes and micro-tubes by Tam *et al*. [28] and Kandlikar *et al.* [19], where the relative surface roughnesses were based off of the R_a parameter for direct roughness measurements. The studies of Ghajar *et al.* [21] and Brackbill and Kandlikar [20] in mini- and micro-tubes had relative surface roughnesses that were two orders of magnitude larger than that of the present study, however, these roughnesses were in some manner estimated and therefore represent the idea of effective relative surface roughnesses. The relative surface roughnesses that were previously obtained in macro-tubes [8, 9, 22, 26, 34, 35] using the sand grain diameters are also orders of magnitudes greater than in this study.

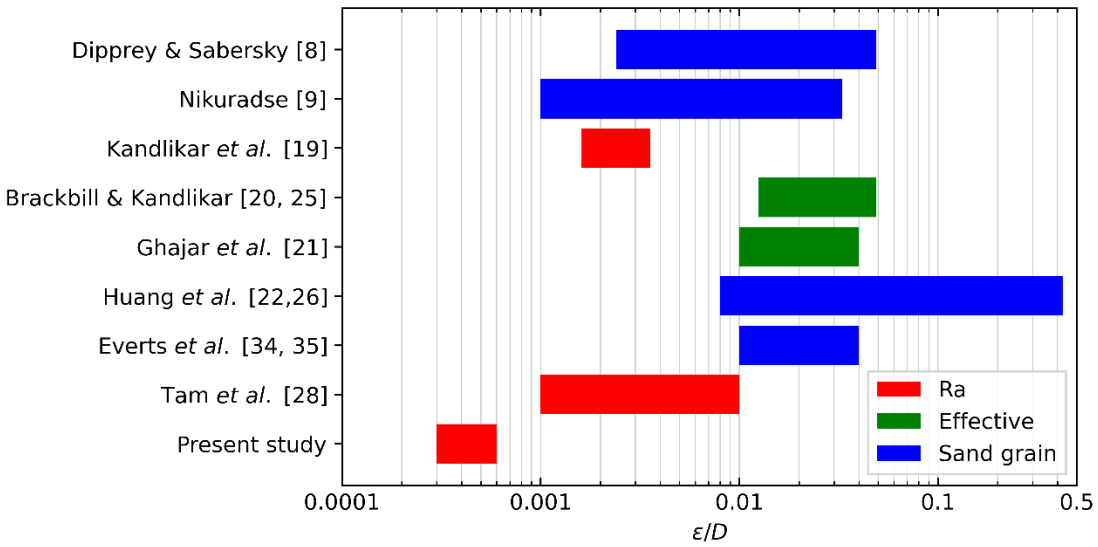

Fig. 1: Summary and comparison of relevant relative surface roughnesses from literature.

This raises two questions. Firstly, why are such low surface roughnesses investigated; surely, the pressure drops and heat transfer rates should be similar than that of a smooth tube? The answer to this question is that the results of this study show that even these small changes lead to noticeable changes in heat transfer and pressure drop.

Secondly, do relative surface roughnesses of the order of magnitude presented in this study, occur in practice? For the second concern it should be noted that the two relative surface roughness values of 0.0003 and 0.0006 were prominent enough to feel with one's finger tips. These roughnesses represent values which could be a result of etching, fouling or scaling. Sandpaper has been used in previous studies to roughen surfaces, as seen in the work of Brackbill and Kandlikar [20, 25] and Young *et al.* [37]. Sandpaper is classified according to grit, where a lower grit number corresponds to a very rough surface – typically used to remove large amounts of material, whilst higher grit number correspond to very fine surfaces – typically used to polish and refine surfaces. The surface roughness values compare well to 2 400 grit and 1 200 grit for the tubes with relative surface roughness of $\varepsilon/D = 0.0003$ and $\varepsilon/D = 0.0006$, respectively. The surface roughness values presented in this study, therefore, represent a practical range of surface roughnesses.

The purpose of this study, therefore, was to experimentally investigate and quantify the effects of surface roughness on the pressure drop and heat transfer characteristics in the laminar and transitional flow regimes in horizontal macro-scale tubes. Furthermore, when considering the relatively short test section lengths used previously, previous studies to date considered the heat transfer and pressure drop characteristics of developing flow through rough tubes, while this study specifically focusses on fully developed flow.

2. Experimental Setup

The layout of the experimental setup which was used to perform the experiments is shown in Fig. 2 and was of the closed-loop configuration. Water, maintained at 20 °C in a 260 ℓ storage tank (1), was pumped through a test section using an electronically controlled positive displacement pump. The water in the storage tank was continuously pumped through a filtration loop to capture any solid particles and mix the water in the tank.

The temperature of the water in the storage tank was controlled using a thermostat-controlled bath (2), with a heating capacity of 3.5 kW and a cooling capacity of 0.9 kW. The water was

pumped through the water loop which included an accumulator (3), a back-pressure valve (4) and a bypass valve (5). The accumulator was used to minimise the flow pulsations from the pump. The back-pressure valve was used to ensure that the pump ran at high revolutions per minute while the pump and accumulator were maintained at high pressures. The bypass valve allowed for the control of the fraction of water which flowed to the mass flow meters (6) and back to the storage tank. During experiments, the pump speed, back-pressure valve and the bypass valve positions were adjusted to allow for steady pre-selected mass flow rates with minimal pulsations to enter the flow meters and the test section (7) [38].

Two Coriolis mass flow meters with different capacities were installed in parallel to account for the wide range of mass flow rates which were tested. After the flow meters, the fluid flowed through an inlet mixer (8), where the mean inlet temperature was measured using an inlet Pt100 probe (9), to the flow-calming section (10), the test section, the outlet mixer (11), where the mean outlet temperature was measured by the outlet Pt100 probe (12), and then back into the storage tank.

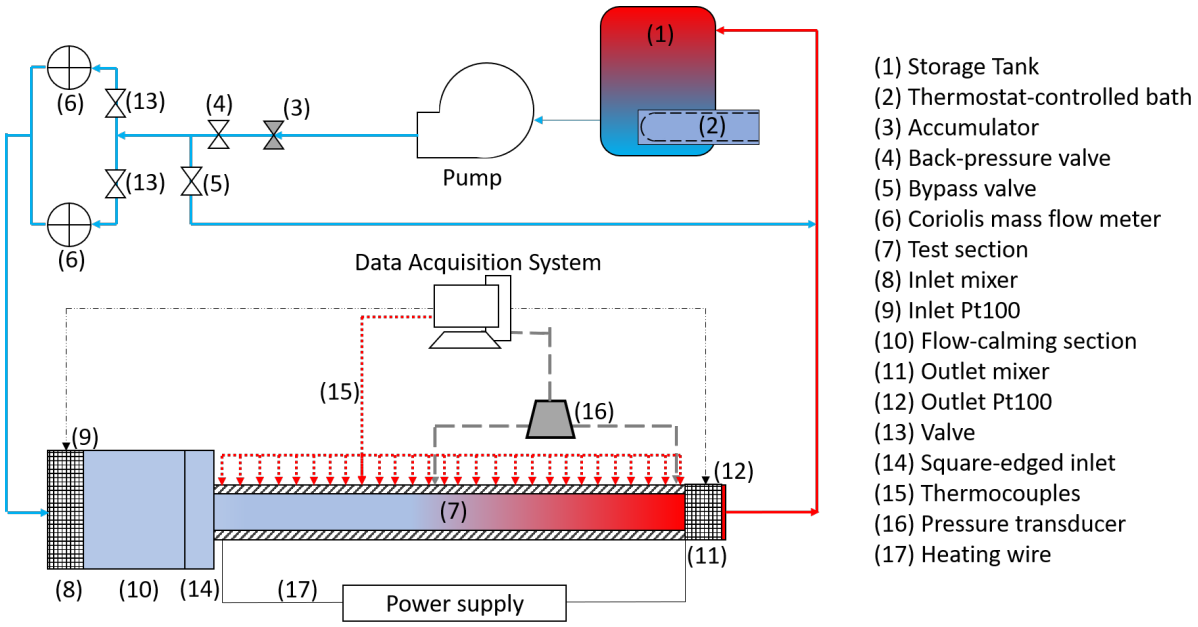

Fig. 2: Schematic of the experimental setup used to conduct the heat transfer and pressure drop experiments.

2.1. Flow-calming section

A flow-calming section (6), similar to the ones used by Ghajar and co-workers [39-42] and Meyer and co-workers [3, 29, 30, 38, 43, 44], was installed downstream of the inlet mixer to straighten the flow prior to entering a test section. The flow-calming section was manufactured using a clear acrylic tube to allow for the easy detection of air bubbles and was insulated to prevent heat loss. The flow-calming section was bolted onto an acetal disk which allowed for the connection to the test section with a square-edged configuration.

2.2. Test section

The test section which was used was that of a hard-drawn copper tube with a mean measured inside diameter of 5.14 mm and an outside diameter of 6.35 mm (Vernier calliper), and a length of 5.45 m (measuring tape). The test section was equipped with 25 thermocouple stations (Fig. 3) spaced axially along the tube length. To detect free convection effects, each thermocouple station contained a thermocouple at the top and bottom, whilst the third thermocouple was

placed 90° from either the top or the bottom thermocouple and alternated every station. The thermocouples were attached to the test section by drilling small indentations into the surface of the tube and inserting solder into the indentations.

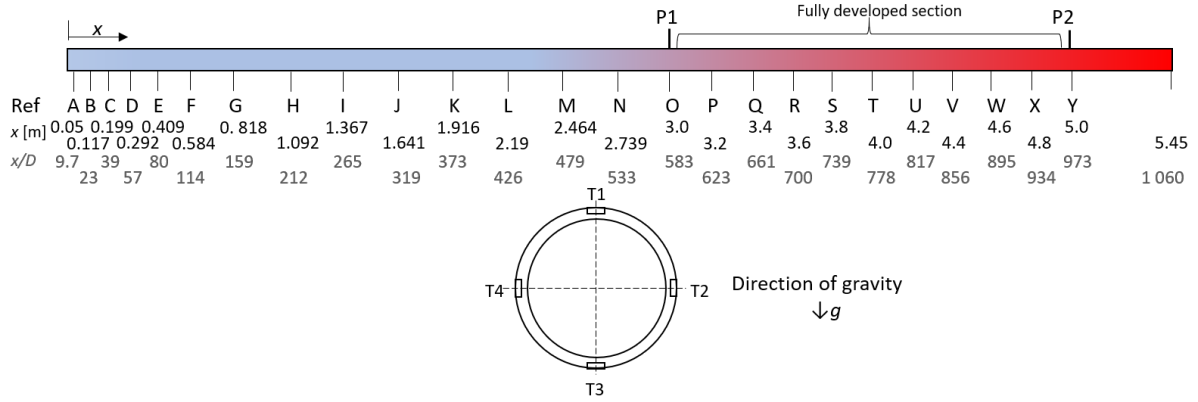

Fig. 3: Schematic of the axial positions and length-to-diameter ratios, *x/D*, of the 25 thermocouple stations, A through Y, and the pressure tap positions, P1 and P2. A cross-section of the test section depicts the positions of the peripheral thermocouples.

Special limits of error T-type thermocouples with a wire diameter of 0.25 mm and an accuracy of 0.1 °C were used. The thermocouples were calibrated in situ between temperatures of 15 °C and 65 °C (using 2.5 °C increments) to ensure they were within limits. The test section was connected to a thermostat-controlled bath which pumped water through the inlet mixer, test section and the outlet mixer, while the inlet and outlet Pt100 probes recorded the reference temperatures.

Two pressure taps, P1 and P2, (as shown schematically in Fig. 3) were attached to the test section for pressure drop measurements. The diameter of the holes for the pressure taps adhered to the specification provided in Rayle [45, 46], which states that the diameter of the orifice must be less than 10% of the inner tube diameter. This prevented localised eddies from disturbing or altering the pressure drop measurements. Pressure measurements were taken using a differential pressure transducer (16) utilising 1.4 kPa, 14 kPa and 22 kPa diaphragms. The diaphragms were calibrated from 0 Pa to their own respective maximum pressure, and had accuracies of 3.5 Pa, 35 Pa and 55 Pa, respectively.

The flow regime maps of Everts and Meyer [44] were used to determine whether forced or mixed convection conditions existed. Furthermore, the position of the first pressure tap was determined using the recently developed equation (based on experimental data) for the mixed convection thermal entrance length [47], shown by Eq. (1). For mixed convection conditions, Everts and Meyer [47] found that the thermal entrance length decreased when compared to pure forced convection, Lt_{FC}. Therefore, by placing the first pressure tap beyond the theoretical thermal entrance for mixed convection, ensured that the flow was fully developed given mixed convection conditions.

$$Lt_{FD} = Lt_{FC}\left(1 - \frac{Gr^{0.1}}{Pr^{0.5}Re^{0.07}}\right) \tag{1}$$

where $Lt_{FC} = 0.12RePrD$ for forced convection conditions. A constant heat flux was applied using electrical heating. The outer surface of the test section was tightly coiled with two insulated constantan wires, with a diameter of 0.38 mm, connected in parallel to the direct current power supply. The wire was coiled in accordance with Everts [38], which concluded

that a gap of 1 mm between the thermocouple and the heating wire was sufficient to maintain a constant heat flux without affecting the temperature measurements.

A full set of smooth test section experiments were performed, both for validation and for comparative purposes, before the test section was roughened for the experiments of this study. The smooth test section's mean surface roughness, ε, was measured with a surface roughness tester as 0.215 µm. The corresponding relative surface roughness, ε/D, was therefore 4.17×10^{-5} and was for the purposes of this study considered to be a smooth tube with $\varepsilon/D \approx 0$.

Once the smooth test section experiments were completed, the test section was disconnected from the experimental setup. The test section was then sand-blasted using platinum grit with grain sizes of 0 to 0.6 mm. The surface roughness was recorded with a Mitutoyo SJ210 surface roughness tester, with an accuracy of 0.002 µm, where the inner tube surface roughness was measured linearly in the flow direction, like Kandlikar [15]. The ISO 4287: 1997 surface profile measurement standard was used and the experimental results obtained indicated that the mean roughness, R_a, correlated better with the Colebrook equation [23]. This resulted in a mean surface roughness of 1.7 µm and a corresponding relative surface roughness of 0.0003.

To measure the roughness of the tube, the tube had to be destructively sectioned through its centre so the probe of the tester could travel along the inner surface of the tube (Fig. 4). The roughness could not be measured in the circumferential direction due to the small diameter of the tube and the larger size of the roughness tester probe.

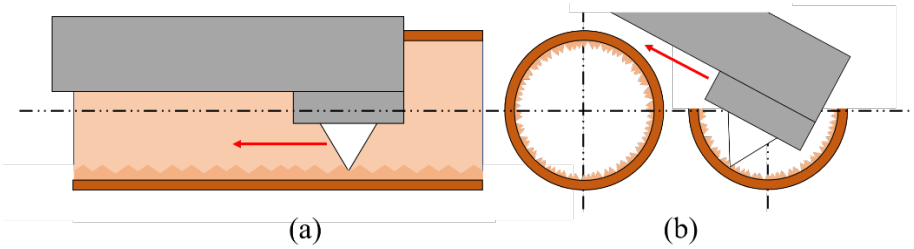

Fig. 4: Surface roughness profile measurement in the (a) flow direction and the (b) circumferential direction.

Preliminary tests were performed to check the consistency and repeatability of the sand blasting of the test section. Tubes were sandblasted to test the dependency of: time blasted, sand grain used, length of tube used, and direction of blasting. To ensure that the roughness was consistent along the 5.5 m-tube length, measurements were taken at 10 equally spaced positions along the tube length. The roughness of the tube was then taken as the average of the ten measured values.

Since the roughness of the tube can only be determined by sectioning the tube into pieces, the roughness of the specific tube being tested had to be measured by using a duplicate tube which followed the exact same blasting technique. The measured R_a roughness values deviated by a maximum of 14% along the tube, excluding the inlet and outlet points which reached a maximum of 42% due to the exit effects of having the tube open to atmosphere. To ensure that the portions of the test section where larger deviations were detected were not taken into consideration, the heat transfer and pressure drop characteristics were only investigated in the fully developed region (between points P1 and P2 in Fig. 3). However, it should be noted that the test section had a slightly increased roughness near the inlet, which could affect the development of the thermal and hydrodynamic boundary layers.

On completion of the experiments using the first rough test section, the test section was again disconnected from the experimental setup and sand-blasted with a larger grain size platinum

grit of 1.0 to 1.2 mm. The mean measured surface roughness was measured to be 3.1 μm and had a corresponding relative surface roughness of 0.0006. The internal diameters of the two roughened tubes were re-measured after sand blasting with the respective sand grits, and were measured as 5.185 mm and 5.20 mm for the first and second rough test sections, respectively. These changes in diameters were taken into consideration with the calculation of the two relative surface roughness values, as well as in the data reduction method.

2.3. Instrumentation

2.3.1. Power supply

A direct current (DC) power supply, with maximum power output of 3 kW, voltage output of 360 V, and current output of 30 A, was used to heat the test section. The power supply allowed for an accuracy of 0.2% of the nominal value for both the measured voltage and current values.

2.3.2. Flow meters

Two Coriolis mass flow meters were used to cover the entire measurement range. The CMF010 flow meter had a maximum flow rate of 108 ℓ/hr and was used for the lower Reynolds number experiments, while the CMF025 flow meter, with a maximum flow rate of 2 180 ℓ/hr, was used for the turbulent experiments. The accuracy of the flow rates was given as 0.05% of the full scale of the flow meter, resulting in an accuracy of 0.054 ℓ/hr and 1.09 ℓ/hr, respectively.

2.3.3. Control and data logging

The data from the experiments was collected through the use of a personal computer with the help of a data acquisition system. The data was recorded using National Instruments LabVIEW software and processed through a personal computer using MathWorks MATLAB scripts.

3. Data Reduction

The mean inlet temperatures, T_i, and mean outlet temperatures, T_e, to the test section were measured by the Pt100 probes. The bulk fluid temperatures, T_b, were calculated as the arithmetic mean of the inlet and outlet temperatures.

$$T_b = \frac{T_i + T_e}{2} \tag{2}$$

The mean fluid temperatures, T_m, at any point, x, along the tube with heated length, L_h, under a constant heat flux boundary condition, increases linearly along the tube length from the mean inlet temperature to the mean outlet temperature.

$$T_m = \left(\frac{T_e - T_i}{L_h}\right) x + T_i \tag{3}$$

At each thermocouple station (Fig. 3) the average surface temperatures, T_s, were calculated by the arithmetic mean of four thermocouples per station, where the thermocouples were situated at the top (T_1), bottom (T_3), left (T_4) and right (T_2) of the cross section (Fig. 3) of the test section. This study, however, used three thermocouples per station where only one thermocouple was either on the left (T_4), or right (T_2) of the tube cross section. Thus, the average outer surface temperature was calculated as the sum of the top, bottom and twice the side thermocouple (T_2 or T_4) and divided by four (thus assuming $T_2 = T_4$). This was to account for the effect of free convection on the peripheral temperature differences.

$$T_{s,i} = \frac{T_1 + T_3 + 2T_2}{4} \quad \text{or} \quad T_{s,i} = \frac{T_1 + T_3 + 2T_4}{4} \tag{4}$$

The average fully developed surface temperatures (between the pressure taps P1 and P2, separated by the length, L), was determined using the following equation:

$$T_s = \frac{1}{L}\int_{L_1}^{L_2} T_{s,i}(x)\,dx \tag{5}$$

With the bulk and mean fluid temperatures and the average surface temperatures calculated, the following properties of water were determined using equations for the thermophysical properties for liquid water [48]: density, ρ, dynamic viscosity, μ, specific heat, C_p, thermal conductivity, k, Prandtl number, Pr, and volumetric thermal expansion coefficient, β. When average fluid properties were required, the bulk temperature from Eq. (2) was used; when the local or fully developed properties were required, the mean fluid temperature from Eq. (3) at the appropriate point, x, was used.

The mass flow rates, $\dot{m}$, were calculated from the products of the water densities, ρ, and the volumetric flow rates, $\dot{V}$, which were measured by the Coriolis mass flow meters.

$$\dot{m} = \rho\dot{V} \tag{6}$$

The Reynolds number was calculated by:

$$Re = \frac{4\dot{m}}{\mu\pi D} \tag{7}$$

The rate of heat transferred, $\dot{Q}_w$, to the water was calculated as:

$$\dot{Q}_w = \dot{m}C_p(T_e - T_i) \tag{8}$$

The rate of electrical heat input, $\dot{Q}_e$, applied to the tube was recorded directly from the power supply to the data acquisition system. The rate of heat transferred to the water, $\dot{Q}_w$, and the rate of the electrical heat input, $\dot{Q}_e$, applied to the tube, should be equivalent in ideal circumstances, however, due to heat losses, small differences are measured. This difference is quantified by the energy balance error, EB, which was used to monitor heat losses.

$$EB = \left[\frac{\dot{Q}_e - \dot{Q}_w}{\dot{Q}_e}\right] \times 100 \tag{9}$$

The energy balance errors of all the experiments were found on average to be 6.4%. Due to heat losses, the rates of heat transferred to the water was used for the subsequent calculations, as the electrical power applied to the test section was deemed to be a less accurate indicator of heat transfer rate.

The heat fluxes, $\dot{q}$, transferred to the water were calculated using the rates of heat transferred to the water, $\dot{Q}_w$, over the surface area, A_s, using the inner tube diameter, D, and test section heated length, L_h:

$$\dot{q} = \frac{\dot{Q}_w}{A_s} = \frac{\dot{m}C_p(T_e - T_i)}{\pi D L_h} \tag{10}$$

With the average surface temperatures, T_s, the mean fluid temperatures, T_m, and the heat fluxes, $\dot{q}$, known, the heat transfer coefficients, h, were determined.

$$h = \frac{\dot{q}}{T_s - T_m} \tag{11}$$

The Nusselt numbers, *Nu*, were calculated with Eq. (12), where, *k*, was the thermal conductivity of the water.

$$Nu = \frac{hD}{k} \tag{12}$$

The difference in temperature, ΔT, across the tube wall was calculated using the heat conduction equation for a cylinder, with D_o the outer diameter of the tube, D the inner diameter of the tube, and k_t the copper tube's thermal conductivity (401 W/m.K [23]).

$$\Delta T = \dot{Q}_w \frac{\ln(D_o/D)}{2\pi k_t L_h} \tag{13}$$

At the highest measured rate of heat transfer to the water of 273 W, the largest temperature difference over the tube wall was calculated to be 0.0041 °C. Due to this temperature difference being significantly smaller than the accuracy of the thermocouples (0.1 °C), it was assumed that the temperature difference over the tube wall was negligible. The measured outer surface temperatures were therefore considered to be equal to the inner surface temperature.

Since the fully developed pressure drops, ΔP, were measured over a length, *L* (between the two pressure taps P1 and P2 shown in Fig. 3), the friction factors, f, were a mean value over the length that the pressure drop measurement was taken.

$$f = \frac{\Delta P \rho D^5 \pi^2}{8\dot{m}^2 L} \tag{14}$$

To determine the Grashof numbers, *Gr*, Eq. (15) was used, where the gravitational acceleration constant, *g*, was taken as 9.81 m/s². The kinematic viscosities, υ, were determined from the viscosities and densities, by $\upsilon = \mu/\rho$.

$$Gr = \frac{g\beta(T_s - T_m)D^3}{v^2} \tag{15}$$

The Rayleigh numbers, *Ra*, were calculated multiplying the Grashof numbers with the Prandtl numbers.

$$Ra = GrPr \tag{16}$$

When the Grashof numbers were multiplied with the Nusselt number, the modified Grashof numbers, Gr^*, were attained. The modified Grashof numbers were therefore a function of heat flux rather than the difference between the surface temperature and the mean fluid temperature.

$$Gr^* = GrNu = \frac{g\beta\dot{q}D^4}{v^2 k} \tag{17}$$

The modified Rayleigh numbers, *Ra**, were calculated as in Eq. (16), using the modified Grashof numbers.

$$Ra^* = Gr^* Pr \tag{18}$$

Finally, the Colburn *j*-factors were calculated as:

$$j = \frac{Nu}{RePr^{1/3}} \tag{19}$$

To determine the flow regime boundaries, the recent equations proposed in Everts and Meyer [29] were used to calculate the critical Reynolds number at which the transitional flow regime starts (Re_{cr}), the start of the quasi-turbulent flow regime (Re_{qt}), the start of the turbulent flow regime (Re_t), the width of the transitional flow regime (ΔRe), and the transition gradient (TG_j). Although these equations were developed for smooth tubes, it should be noted that most studies generally determine the flow regime boundaries through visual inspection and can result in the flow regime boundaries being subjectively defined. Thus, rather than identifying the transition metrics by visual inspection alone, the methodology and rationales proposed by Everts and Meyer [29] were used as a guideline and confirmed through visual inspections. These equations are given in Eqs. (20)-(24) and were obtained from the Reynolds numbers, Colburn *j*-factors, and Nusselt numbers.

$$Re = Re_{cr} \; when \left(\frac{dj}{dRe}\right)_{i-2:i} = 0 \tag{20}$$

$$Re = Re_{qt} \; when \left(\frac{d^2Nu}{dRe^2}\right)_{i:i+2} \geq -0.00015 \tag{21}$$

$$Re = Re_t \; when \left(\frac{dNu}{dRe}\right)_{qt} = \left(\frac{dNu}{dRe}\right)_t \tag{22}$$

$$\Delta Re = Re_{qt} - Re_{cr} \tag{23}$$

$$TG_j = \frac{j_{qt} - j_{cr}}{Re_{qt} - Re_{cr}} \tag{24}$$

4. Uncertainties

The methodology used to determine the uncertainties of the measured and calculated quantities was described by Dunn [49], where all standard deviations for the sample size of 200 data points were calculated and multiplied with the Student's *t*-variable such that the confidence that the true value lies within the uncertainty interval was 95%. Examples of the calculations of the uncertainty analysis can be found in the work of Everts [38, 50] as well as Everts and Meyer [51].

The ranges of the instrumentation used are summarised in Table 1, along with the error of the instrument and the calibrated uncertainties. For the pressure drop measurements, DPT indicates the three different differential pressure transducers that were used, and for the flow rate measurements, CMF indicates the two different Coriolis flow meters that were used. The error of the measured physical dimensions, as well as the thermophysical properties of water that were used in the data reduction (Section 3), are given in Table 2.

Table 1: Ranges, accuracies and calibrated uncertainty of the instrumentation used

Instrument	Range	Error	Calibrated uncertainty
Temperature measurements			
Pt100	-100 to 250 °C	0.06 °C	0.031 °C
T-type thermocouples	-250 to 260 °C	0.1 °C	0.072 °C
Pressure drop measurements			
DPT 1.4 kPa	0 to 1.4 kPa	3.5 Pa (0.25% of FS)	2.55 Pa
DPT 14 kPa	0 to 14 kPa	35 Pa (0.25% of FS)	25.4 Pa
DPT 22 kPa	0 to 22 kPa	55 Pa (0.25% of FS)	28.9 Pa
Flow rate measurements			
CMF010	0 to 108 ℓ/hr	0.05% of FS	-
CMF025	0 to 2180 ℓ/hr	0.05% of FS	-
Input power			
Current	0 to 30 A	0.02% of the value	-
Voltage	0 to 360 V	0.02% of the value	-

Table 2: Ranges and accuracies of physical dimensions and fluid properties.

Measurement	Range	Error
Dimensions		
D and D_o	-	0.02 mm
L and L_h	-	0.001 m
Fluid properties		
ρ	0 to 150 °C	0.004% of the value
μ	0 to 150 °C	1% of the value
C_p	0 to 150 °C	0.04% of the value
k	0 to 150 °C	2% of the value

Through the principle of the propagation of uncertainty, the uncertainties of the calculated quantities presented in the data reduction, were determined. The uncertainties in the Reynolds numbers were a maximum of 1.8% at a Reynolds number of 400 and decreased with increasing Reynolds numbers to 1.1% at a Reynolds number between approximately 6 000 to 7 500. When switching to the higher capacity Coriolis flow meter, the uncertainties in the turbulent flow regime increased to a maximum of 1.8%. The uncertainties of the friction factors were less than 4.5% in the laminar flow regime, which increased in the transitional flow regime to a maximum of 7.5% and decreased in the quasi-turbulent and turbulent flow regime to less than 3.5%.

For the highest heat flux of 3 kW/m², the uncertainties of the average Nusselt numbers in the laminar flow regime were less than 3.1% and increased with increasing Reynolds numbers to a maximum of 14% in the turbulent flow regime. When the heat flux was decreased to the minimum of 1 kW/m², the average Nusselt number uncertainties in the laminar and turbulent flow regimes increased to a maximum of 7.2% and 35%, respectively. At Reynolds numbers lower than 6 000 this reduced to 25%. For laminar forced convection conditions (at a heat flux of 1 kW/m²), the average Nusselt number uncertainty was 4.3%.

5. Experimental Procedure and Test Matrix

The experiments that were performed are summarised in Table 3. The smooth tube (S) results were used as validation with literature and as baseline tests for comparison with the rough tubes. Thereafter experiments were performed on two rough tubes (R1 and R2) with relative surface roughness, ε/D, values of 0.0003 and 0.0006.

The smooth and two rough tubes were tested at heat fluxes of 0 (isothermal), 1, 2 and 3 kW/m^2. As shown in Table 3, 192 different Reynolds number tests were performed on the smooth tube, 194 tests on the intermediate roughness tube and 188 tests on the roughest tube, resulting in a total of 574 mass flow rate measurements, 44 198 temperature measurements and 665 pressure drop measurements.

Table 3: Experimental test matrix for this study

Test section	**Naming convention**	**Heat flux, $\dot{q}$ [kW/m^2]**	**Relative surface roughness, ε/D**	**Number of Re increments**
Smooth	S	0	~ 0	50
		1	~ 0	52
		2	~ 0	46
		3	~ 0	44
Intermediate roughness	R1	0	0.0003	48
		1	0.0003	51
		2	0.0003	49
		3	0.0003	46
Roughest	R2	0	0.0006	51
		1	0.0006	46
		2	0.0006	44
		3	0.0006	47
Total				574

Experiments began once the temperatures in the entire system had reached 20 °C. The Reynolds number was set to approximately 7 000 and the thermostat-controlled bath to 20 °C. The system took between 2 hours and 5 hours to reach a steady temperature of 20°C, depending on the ambient temperature of the laboratory for the specific day. Once the system temperature stabilized at 20 °C, the mass flow rate was decreased until an appropriate pressure drop was obtained, to allow for the safe connection of the required differential pressure transducer. The mass flow rate was then increased to the maximum flow rate for the Reynolds number range, which was to be tested, corresponding to 9 800 for turbulent, 7 100 for quasi-turbulent and transitional, and 2 100 for laminar flow.

Steady state conditions were considered met once there were no variations in temperatures for the inlet and outlet Pt100 probes over a 15-minute period. Generally, steady state was achieved after 30 minutes in the laminar and turbulent flow regimes. In the transitional flow regime, steady state was achieved anywhere between 30 minutes to 1 hour.

Once steady state conditions were achieved for the desired Reynolds number, 200 data points of all the temperatures, mass flow rates, power output and pressure drop measurements were logged at a frequency of 20 Hz. The 200 data points were then averaged and considered as a singular value for each thermocouple station, mass flow rate and pressure drop measurement.

6. Validations

To confirm that the experimental setup, methodology, and data reduction was valid and accurate, the results obtained using the smooth tube were compared to equations from literature.

6.1. Fully developed isothermal friction factors

The fully developed isothermal friction factors were validated in Fig. 5 by comparing the experimental data in the laminar and turbulent flow regimes to the Poiseuille [23] and the Blasius [52] equations, respectively. The validations were performed with 52 data points, with the Reynolds numbers ranging from 500 to 10 000 to ensure both flow regimes were tested over the 2 m fully developed part ($583 \leq x/D \leq 972$) of the tube (Fig. 3).

The laminar fully developed friction factors correlated well with the Poiseuille equation for fully developed flow, with deviations up to 3% between Reynolds numbers of 500 and 2 000. The turbulent friction factors correlated well with the Blasius equation with deviations of up to 6% for Reynolds numbers between 3 000 and 10 000.

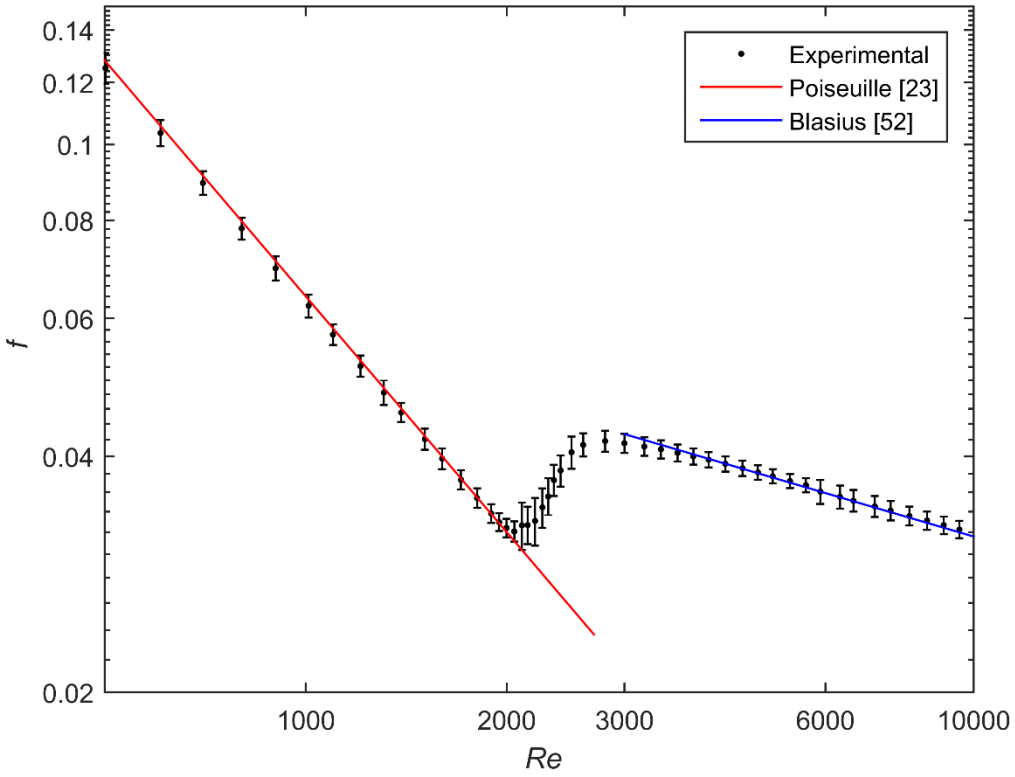

Fig. 5: Validation of the fully developed isothermal friction factors in the laminar and turbulent flow regimes with the Poiseuille [23] and the Blasius [52] equations, respectively.

6.2. Local laminar Nusselt numbers for forced convection

The laminar forced convection Nusselt number validation was performed by comparing the local Nusselt numbers to the equation of Shah and London [53] and the analytical solution $Nu = 4.36$ [23], for fully developed laminar flow given a constant heat flux boundary condition. Fig. 6 contains the local Nusselt numbers at a bulk Reynolds number of 403 and heat flux of 1 kW/m² as a function of the dimensionless length-to-diameter ratio. The experimental data correlated well with the equation of Shah and London [53] with an average deviation of 8.2%.

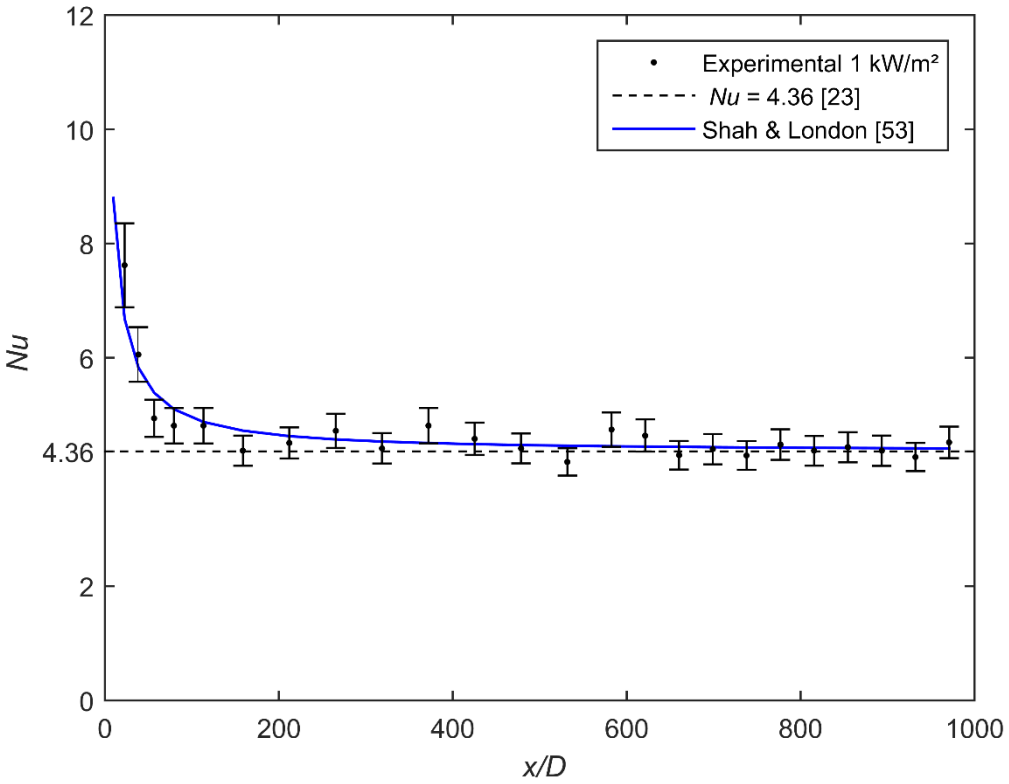

Fig. 6: Validation of the local laminar Nusselt numbers for forced convection conditions at a Reynolds number of 401 and a heat flux of 1 kW/m².

The average Nusselt number in the fully developed region was 4.45 and therefore within 2% of the analytical value of 4.36 [23], which is represented by the dashed black line.

6.3. Local Nusselt numbers for mixed convection

The equations developed by Meyer and Everts [43] and Morcos and Bergles [54] were used in Fig. 7 for the validation of the laminar Nusselt numbers at a bulk Reynolds number of approximately 1 000 and a heat flux of 3 kW/m². The experimental data deviated from the equation of Morcos and Bergles [54] on average by 15.3%. However, between $x/D = 57$ and $x/D = 972$, where the Nusselt numbers became relatively flat as the flow became fully developed, the deviation reduced to 5.3%. This was because the equation was developed for fully developed flow and not developing flow. The local Nusselt numbers correlated well with the equation of Meyer and Everts [43] with an average deviation of 6.8%.

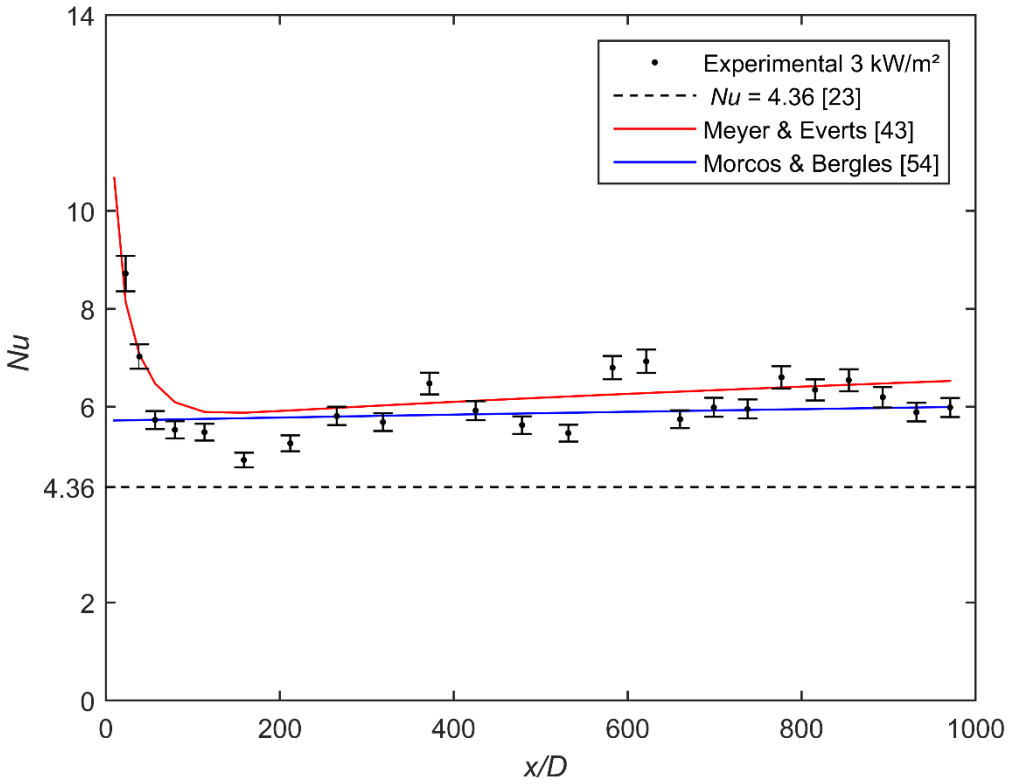

Fig. 7: Validation of the local laminar Nusselt numbers for mixed convection conditions at a Reynolds number of 1 000 for the 3 kW/m² heat flux.

6.4. Average fully developed Nusselt numbers for mixed convection

In Section 6.3 it was confirmed that mixed convection conditions were achieved for the 3 kW/m² heat flux. Between the Reynolds numbers of 800 and 1 800, the thermal entrance lengths were calculated to be between 0.93 m and 3.36 m (x/D = 181 and x/D = 654). At higher Reynolds numbers in the laminar flow regime, the entrance lengths extended into the fully developed part ($583 \leq x/D \leq 972$ in Fig. 3) of the tube. However, since only a small portion of this region contained developing flow and the Nusselt numbers asymptotically reached the fully developed values, it was assumed that this small portion of tube containing developing flow had a negligible effect on the average Nusselt numbers calculated over the entire fully developed region. In the turbulent flow regime, the flow became thermally fully developed approximately ten diameters from the inlet.

6.4.1. Laminar flow

For the 3 kW/m² heat flux, the average laminar Nusselt numbers between the Reynolds numbers of 800 and 2 000, were validated using the equations of Meyer and Everts [43] and Morcos and Bergles [54] in Fig. 8. The experimental data correlated well with the equations of Morcos and Bergles [54] and Meyer and Everts [43], where the average deviations were 2.9% and 3.9%, respectively. The deviations were found to be larger at lower Reynolds numbers than at higher Reynolds numbers. The deviations at lower Reynolds numbers, where the flow rates were very low, were probably due to the ambient heat that was transferred into the system, primarily through the flow-calming section.

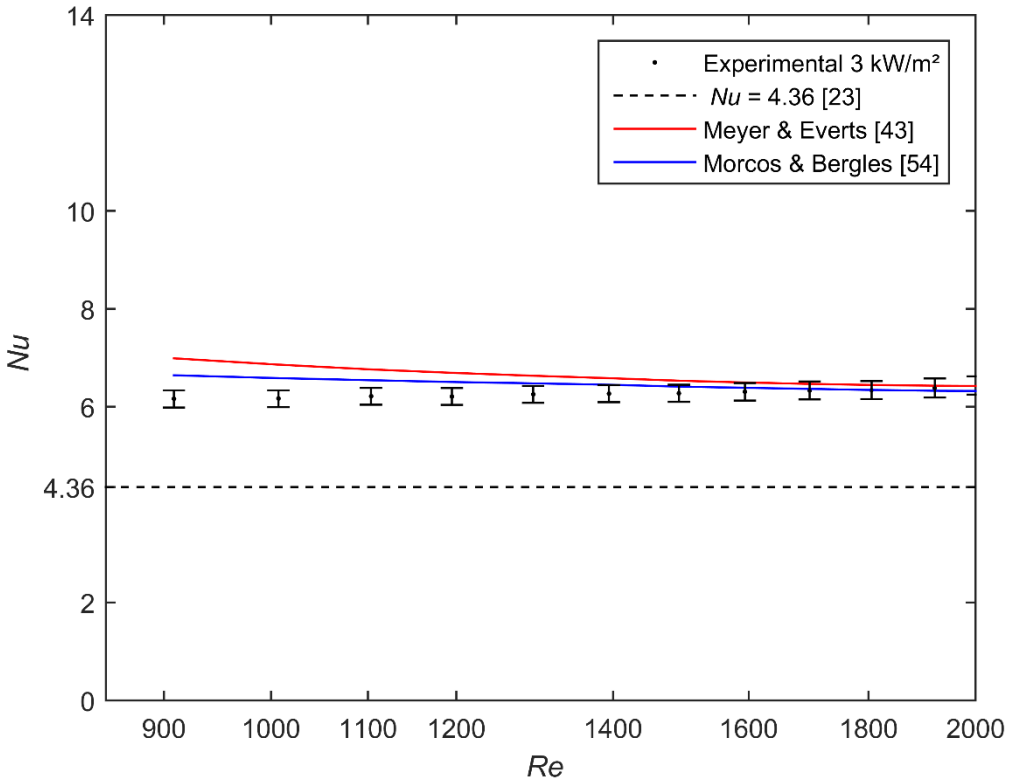

Fig. 8: Validation of the average fully developed laminar Nusselt numbers for mixed convection conditions with equations from literature at a 3 kW/m² heat flux.

6.4.2. Turbulent flow

In the quasi-turbulent and turbulent flow regimes, the average Nusselt numbers in the fully developed region were compared to the newly developed and more accurate equation of Meyer *et al.* [55] and the well-established Gnielinski [56] equation in Fig. 9. A heat flux of 3 kW/m² was applied and the Reynolds numbers varied between 2 600 and 9 900. The equation of Gnielinski [56] was developed for Reynolds numbers above 3 000 and the equation of Meyer *et al.* [55] included Reynolds numbers as low as 2 445.

Despite the experimental data being compliant with the required ranges of the equations, Fig. 9 indicates that the experimental data was significantly lower than both equations, especially at higher Reynolds numbers. The deviation of the experimental data from the equation of Gnielinski [56] was a minimum of 6.2% at a Reynolds number of approximately 2 600 and gradually increased to 36% at the maximum Reynolds number of 9 900. When comparing the experimental data to the equation of Meyer *et al.* [55], the deviation was 15% at a Reynolds number of 2 600 which decreased to a minimum of 11% at Reynolds number of 3 500, and gradually increased to 31% at a Reynolds number of 9 900.

The deviations observed were more prevalent at higher Reynolds numbers. Through a sensitivity analysis, it was found when the difference between the average surface temperatures and the mean fluid temperatures were relatively small (often less than 1 °C at Reynolds numbers above 3 700), the inherent measurement error of the instrumentation and the proximity of the heating coils to the thermocouples, were sufficient to cause deviation of the Nusselt numbers from the equations from literature.

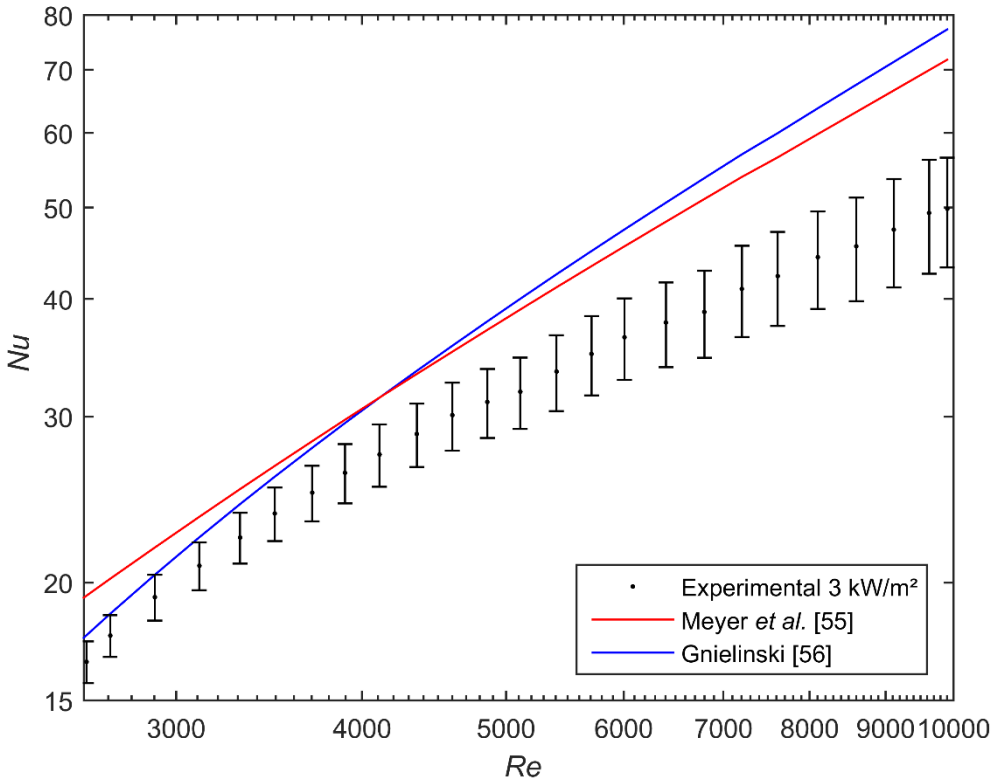

Fig. 9: Validation of the fully developed Nusselt numbers in the quasi-turbulent and turbulent flow regimes with equations from literature for the 3 kW/m² heat flux.

The Nusselt number results had a deviation of more than 10% at Reynolds numbers higher than 3 700, which is in the upper part of the quasi-turbulent flow regime and not the focus of this study. Rather than not showing it in this paper, it is included as it holds qualitative merit by accurately presenting the general trends in the quasi-turbulent and turbulent flow regimes, although it is not necessarily quantitively accurate.

7. Results

7.1. Heat transfer

The effect that the surface roughness has on heat transfer through macro-tubes has received little attention in literature. The fully developed Nusselt numbers for different surface roughnesses are investigated by grouping the results by heat flux in Fig. 10. For fully developed forced convective laminar flow in smooth horizontal tubes, the Nusselt numbers are expected to be approximately 4.36, which is indicated by the dotted black lines. Fig. 10(a) indicates that although the average Nusselt number at a heat flux of 1 kW/m² was 4.94, the Nusselt number was 4.45 at a Reynolds number of 401, which was the case used for the local laminar forced convection validation. The Nusselt numbers increased as the Reynolds number increased. This was attributed to the influence of developing flow, where the laminar forced convection thermal entrance length increases as the Reynolds number increases. At Reynolds numbers above 800, the thermal entrance lengths extended into the fully developed part ($583 \leq x/D \leq 972$) of the tube, indicated in Fig. 3, causing the steady increase of the Nusselt numbers as the Reynolds number was increased further. For Reynolds numbers less than approximately 1 000, Fig. 10(a) indicates this increase due to developing flow was less for heat fluxes of 2 kW/m² and 3 kW/m². Everts and Meyer [47] found that secondary flow decreased

the thermal entrance length, therefore a smaller portion of the developing flow extended into the fully developed region, leading to decreased Nusselt numbers.

When comparing the trends of the laminar Nusselt numbers in Fig. 10(a)-(c) for different heat fluxes, it follows that the magnitude of the Nusselt numbers generally increased with heat flux, due to secondary flow. In the smooth tube, the laminar Nusselt numbers increased approximately parallel from the analytical solution of $Nu = 4.36$, as the heat flux was increased. At a heat flux of 1 kW/m², the average Nusselt number was 4.94, which increased to 5.82 and 6.35 at the 2 kW/m² and 3 kW/m² heat fluxes, respectively.

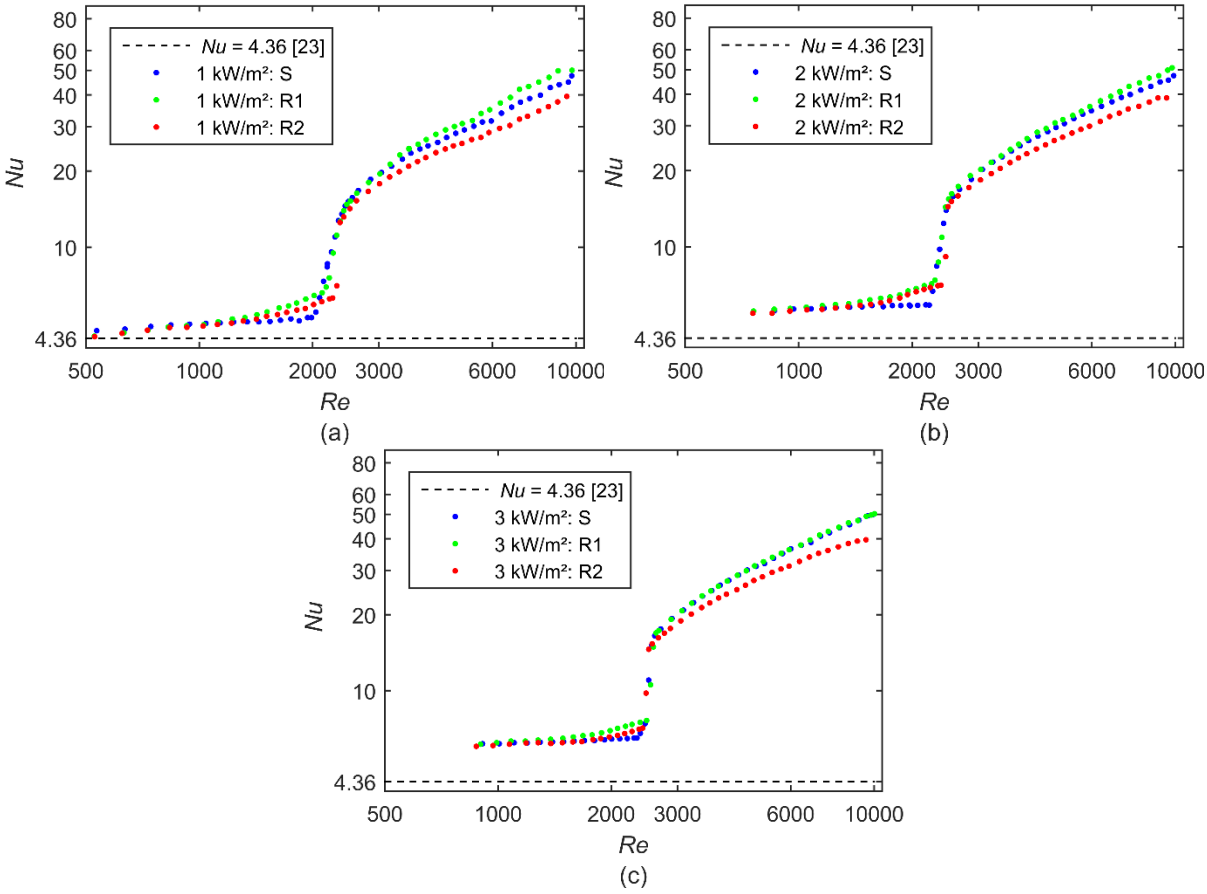

Fig. 10: Comparison of the fully developed Nusselt numbers as a function of Reynolds number for three different relative surface roughnesses at heat fluxes of (a) 1 kW/m², (b) 2 kW/m² and (c) 3 kW/m².

Fig. 10(a) indicates that for Reynolds numbers less than approximately 1 200, surface roughness had a negligible effect on the magnitude of the Nusselt numbers. However, at higher Reynolds numbers near to the critical Reynolds number, an increase in surface roughness caused a gradual increase in the Nusselt numbers. A similar trend was also observed by Celata *et al.* [32] who explained that the surface roughness breaks the laminar hydrodynamic boundary layer and increases the flow resistance. Although not mentioned by Celata *et al.* [32], this graph indicates that the increase in surface roughness disturbed the development of the thermal boundary layer leading to an increased thermal entrance length. As the portion of tube that contained developing flow increased with increasing Reynolds number, the Nusselt numbers increased, because the heat transfer coefficients of developing flow are higher than for fully developed flow.

Another interesting observation from Fig. 10 was that as the surface roughness was increased, the effect of increasing heat flux on the laminar Nusselt numbers decreased. When compared to the smooth tube, the laminar Nusselt numbers in R1 increased by a maximum of 22%, 21% and 15% at heat fluxes of 1, 2 and 3 kW/m², respectively. Although R2 had a higher relative surface roughness, the Nusselt numbers only increased by 13%, 17% and 10% at the respective heat fluxes. More specifically, at a Reynolds number of approximately 2 000, the Nusselt numbers in the smooth tube increased by 22% when the heat flux was increased from 1 kW/m² to 3 kW/m², in the rough tubes this decreased to 7% and 10% for R1 and R2, respectively. There are two possible reasons for this: (1) An increase in surface roughness caused the thermal entrance length to increase and thermal boundary layer thickness to decrease, which led to decreased secondary flow. (2) An increase in Reynolds number reduces the boundary layer thickness near the tube surface, exposing a larger proportion of the boundary layer to the height of the surface roughness profile. Due to the increased exposure of the surface roughness profile, a larger proportion of the boundary layer is subjected to flow disturbances and mixing which dampened secondary flow effects.

From literature [15, 19-21, 25, 27, 28] it was generally found that an increase in surface roughness, caused a decrease in the critical Reynolds number. However, Fig. 10 indicates that the opposite trend was found in this study. At a heat flux of 1 kW/m², the transitional flow regime started at a Reynolds number of 1 986 in the smooth tube and was delayed to Reynolds numbers of 2 119 and 2 259 in R1 and R2, respectively. The critical Reynolds number at which the transitional flow regime started, was expected to increase as the heat flux increased [28, 29, 41, 42], and this trend was observed in Fig. 10, regardless of surface roughness.

Comparing R1 to smooth in the quasi-turbulent and turbulent flow regimes (Reynolds numbers between 3 000 and 9 500), an average increase in the Nusselt numbers of 7.4% was found at 1 kW/m². This reduced to 3.9% at 2 kW/m² and 0.2% at 3 kW/m². Since the increase was significantly higher at a heat flux of 1 kW/m² (where the uncertainties were the highest due to the very small surface-fluid temperature differences) than at 3 kW/m² (where the uncertainties were the lowest), the increase in Nusselt numbers may not only be a direct cause of the surface roughness, but also a symptom of heat losses to the environment. Furthermore, the heat flux had little effect on the fully developed Nusselt numbers in these flow regimes, because secondary flow was suppressed by the velocity of the fluid. The largest deviations in the turbulent Nusselt numbers occurred in the 1 kW/m² results due to the uncertainties related to the very small surface-fluid temperature differences.

When comparing the results of R2 to smooth between Reynolds numbers of 3 000 and 9 500, an unexpected trend was observed. Instead of the expected increase in the Nusselt numbers with increasing relative surface roughness, the Nusselt numbers decreased by an average of 12%, 12% and 13% for the 1, 2 and 3 kW/m² heat fluxes, respectively. Given a specific heat flux and Reynolds number, the mean outer surface temperatures of R2 were larger than those of smooth and R1. A considerable amount of visual deposition (discussed in Section 7.3) was found on the inner surface of the tube, resulting in a thermal resistive layer. This could explain the increase of the measured surface temperatures and therefore the reduced Nusselt numbers in this tube. This explanation also extends to Reynolds numbers greater than approximately 1 000 in the laminar flow regime. The Nusselt numbers increased when compared to the smooth tube, however, when compared to the tube with a lower relative surface roughness (R1) the Nusselt numbers were in fact lower.

7.2. Pressure Drop

The fully developed friction factors for the different relative surface roughnesses are compared in Fig. 11 at different heat fluxes. Classical laminar theory dictates that the friction factors in

the laminar flow regime should equate to $f = 64/Re$ [23], known as the Poiseuille equation, which is represented by the solid black line. In the turbulent flow regime, the friction factors were compared to the Blasius equation [57] for friction factors in smooth tubes. In general, the friction factors decreased with increasing Reynolds numbers with the exception of the transitional and quasi-turbulent flow regimes.

Under isothermal conditions (Fig. 11(a)), the laminar friction factors only deviated from $f = 64/Re$ by 3%, 5% and 6% for the smooth, R1 and R2 tubes, respectively. Although these values correlate very well to classical laminar theory, when comparing each Reynolds number interval, there is a slight increase in the friction factors with increasing surface roughness. From close inspection it follows that the Reynolds number at which the friction factors detach from the Poiseuille equation, decreased with increasing surface roughness. This is in good agreement with the findings of Celata *et al*. [32], namely that the surface roughness breaks up the boundary layers and increases the flow resistance. Previous studies [1, 9, 14, 23] have found that there is little to no effect on friction factors in the laminar flow regime for macro-tubes under isothermal conditions, however, in mini- and micro-tubes it has been found that the surface roughness had an influence on the laminar friction factors [15, 20, 21, 28].

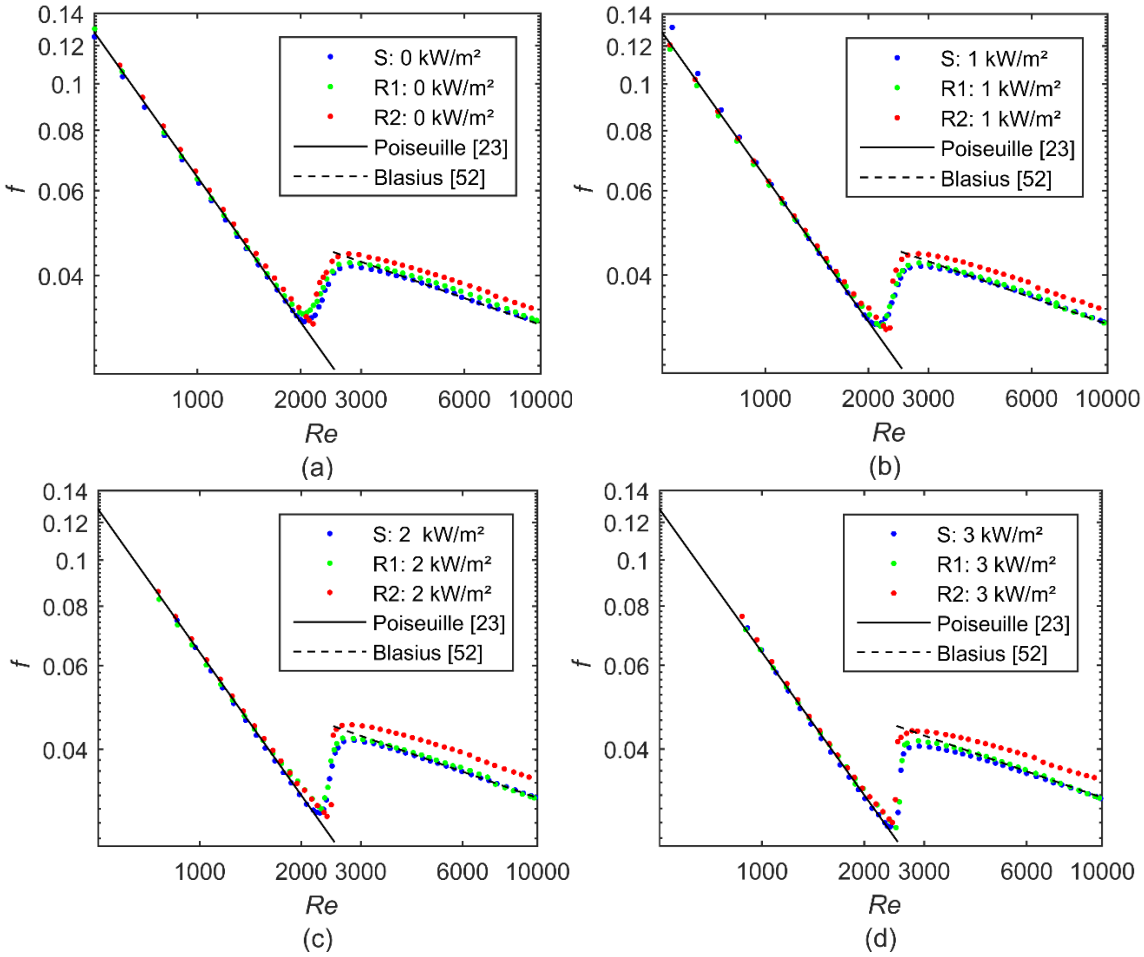

Fig. 11: Comparison of fully developed friction factors as a function of Reynolds number for three relative surface roughnesses at a heat flux of (a) 0 kW/m² (isothermal), (b) 1 kW/m², (c) 2 kW/m² and (d) 3 kW/m².

As expected from previous results obtained by Everts and Meyer [29], an increase in the heat flux caused a delay in the onset of transition due to the increase of temperature, resulting in a decreased viscosity of the test fluid. To clarify the effect of heat flux, the friction factors for each surface roughness are compared for different heat fluxes in Fig. 12(a-c).

The laminar diabatic friction factors in the smooth tube remained within 3% of $f = 64/Re$ for all tested heat fluxes. However, it was observed that the friction factors of the two rough tubes detached from the $f = 64/Re$-line at higher laminar Reynolds numbers. This is in good agreement with the trends observed in the Nusselt numbers in Fig. 10. For R1, the laminar friction factors deviated from $f = 64/Re$ for Reynolds numbers up to 2 076 by a maximum of 5.5%, 5%, 5.1% and 3% for the 0 kW/m^2, 1 kW/m^2, 2 kW/m^2 and 3 kW/m^2 heat fluxes, respectively. For R2, the laminar friction factors for Reynolds numbers less than 2 076, deviated from the Poiseuille equation by a maximum of 7.9%, 8.6%, 7.7% and 5.9% for the 0 kW/m^2, 1 kW/m^2, 2 kW/m^2 and 3 kW/m^2 heat fluxes, respectively. It can therefore be concluded that, similar to the Nusselt number trends, the deviation from $f = 64/Re$ increased with increasing surface roughness, but decreased with increasing heat flux. An increase in heat flux, led to decreased densities and viscosities which in turn led to decreased flow resistances. Observing the same trends in the heat transfer and pressure drop results, are in good agreement with the findings of Everts and Meyer [30], namely that a direct relationship between heat transfer and pressure drop exists in all flow regimes. Therefore, an increase in friction factors is expected to be accompanied by an increase in Nusselt numbers.

The friction factors in R1 (represented by green markers) appeared to be higher throughout the entire Reynolds number range when compared to the smooth tube in Fig. 11(a). However, the R2 friction factors (represented by red markers) decreased below the critical point of the smooth tube in the laminar flow regime (indicating a delay in the start of the transitional flow regime) and then made a sharp and pronounced transition reaching the Blasius equation [52] at a lower Reynolds number than the other tubes. The increase in surface roughness therefore delayed transition and decreased the width of the transitional flow regime.

Similar trends were observed for heat fluxes of 1 kW/m^2 and 2 kW/m^2. However, Fig. 11(d) indicates that at a heat flux of 3 kW/m^2, an increase in heat flux initially delayed the start of the transitional flow regime (R1 compared to smooth), but then the transitional flow regime started at a lower Reynolds number when tested at the maximum roughness (R2) compared to R1. The different behaviour of the 3 kW/m^2 heat flux experiments (which were repeated several times) for R2 was seen as an anomaly. Although the critical Reynolds numbers did not the hold trend, the width of the transitional flow regime and the transition gradient both obeyed the previous trends, decreasing from 172 to 86 and increasing from 4.99×10^{-5} to 14.6×10^{-5}, respectively, when the surface roughness was increased from smooth to R2.

In the quasi-turbulent and turbulent flow regimes, a noticeable increase was observed in Fig. 12 when increasing the surface roughness. When comparing the isothermal data in Fig. 11(a) for Reynolds numbers greater than 3 000 in the smooth tube, the deviation from the Blasius equation [52] was at a maximum of 2%, while an average increase of 2% and 6% from smooth to R1 and R2, respectively, were observed. This was as expected as the Moody Chart [14] also

indicates that an increase in surface roughness has a significant influence on the turbulent friction factors.

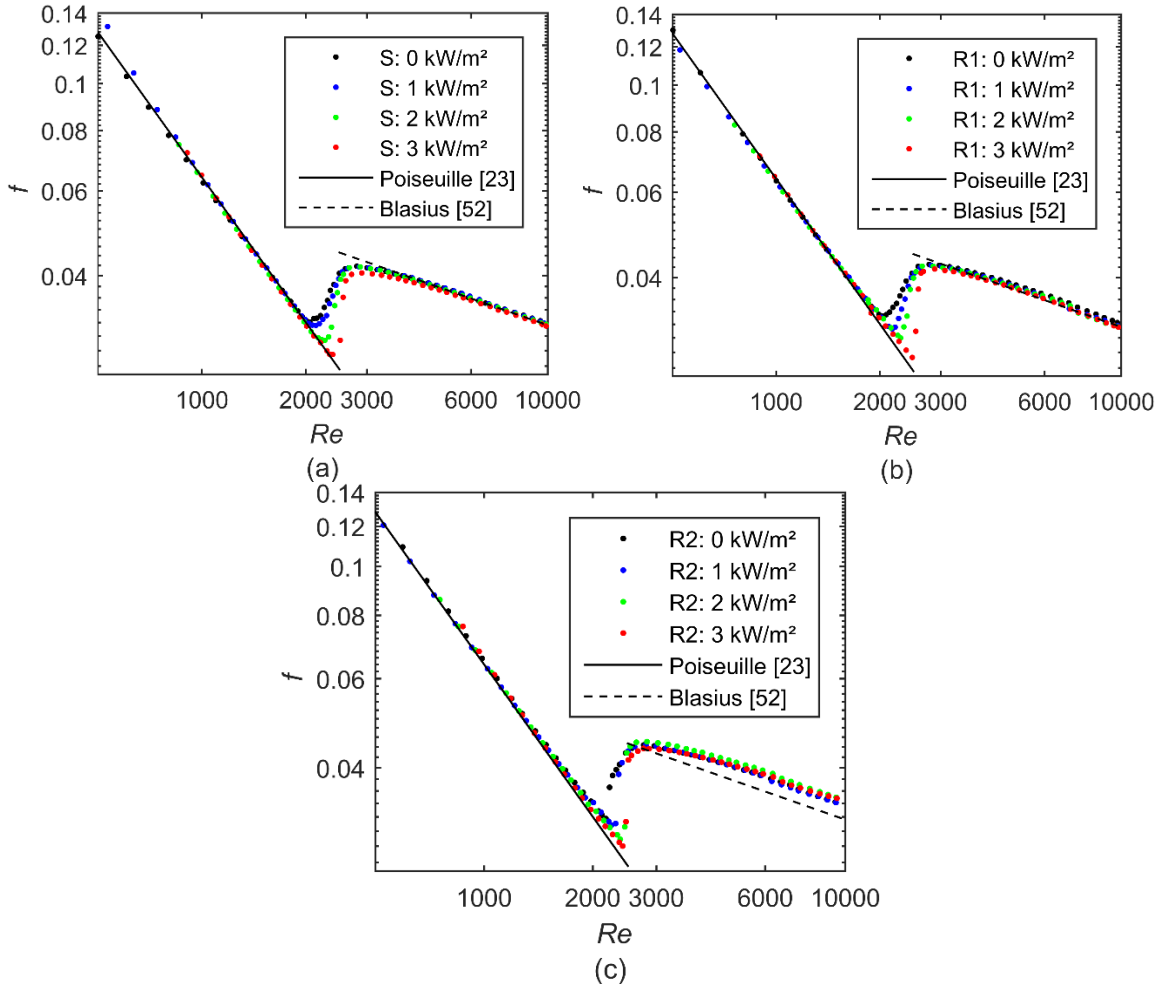

Fig. 12: Comparison of fully developed friction factors at three heat fluxes with respect to the Reynolds number for each set relative surface roughness: (a) smooth tube, (b) R1 and (c) R2.

At a heat flux of 1 kW/m^2, Fig. 11(b) indicates that the surface roughness increased the friction factors in the quasi-turbulent flow regime by up to 4.7% and 9.5% from smooth to R1 and R2, respectively. In the turbulent flow regime, an increase of 6% was found from smooth to R2. Similarly, at heat fluxes of 2 kW/m^2 and 3 kW/m^2, the quasi-turbulent friction factors increased by a maximum of approximately 2-3% and 10% from smooth to R1 and R2, while there was an average increase of 9% in the turbulent friction factors from smooth to R2.

When comparing the magnitudes of the friction factors for different heat fluxes in Fig. 12(a-c), it was found that for the smooth tube in the quasi-turbulent flow regime, the friction factors decreased by a maximum of 3%, 2.8% and 11% from the 0 kW/m^2 (isothermal) experiments to the 1 kW/m^2, 2 kW/m^2 and 3 kW/m^2 heat fluxes, respectively. The maximum deviation occurred at the start of the quasi-turbulent flow regime and became negligible in the turbulent flow regime. This decrease was as a result of an increase in temperature and consequently a decrease in the viscosity of the test fluid. As the Reynolds number increased, the increase in temperature with increasing heat flux decreased, which explains why the effect of increasing heat fluxes decreased in the turbulent flow regime.

Fig. 12 also indicates that as the surface roughness was increased, the effect of heat flux on the quasi-turbulent and turbulent friction factors decreased. For R1, the quasi-turbulent friction factors decreased from the isothermal experiments by up to 2.8%, 5.6% and 3.4% with increasing heat fluxes, while the difference was negligible in the turbulent flow regime. For R2, the quasi-turbulent friction factors decreased by a maximum of 4.3% for both the 1 kW/m^2 and the 3 kW/m^2 heat fluxes, while there was an increase of up to 2.3% at a heat flux of 2 kW/m^2. In the turbulent flow regime, unexpected but slight increases of 2% and 1.3% from the isothermal experiment to the 2 kW/m^2 and 3 kW/m^2 heat fluxes, respectively, were observed.

This was due to a build-up of deposit, as will be explained in Section 7.3. This deposit layer increased the surface roughness and simultaneously acted as a heat resistive layer. As a result, the increases in heat flux were unable to transfer heat through the tube wall as effectively as the smooth and R1 tubes. Consequently, the fluid's temperature increase was limited, which resulted in higher densities and viscosities. An increase in density increases the friction factor while an increase in viscosity decreases the Reynolds number through the inversely proportional relationship.

7.3. Discrepancies for Rough Tube 2

The behaviour of R2 differed significantly from R1, with increasing friction factors and decreasing of Nusselt numbers in the quasi-turbulent and turbulent flow regimes. When analysing the 3 kW/m^2 heat flux experiments, where the uncertainties were the lowest, the following was observed: An increase in relative surface roughness from smooth to R1 (ε/D = 0.0003) increased the friction factor by 2.7% and Nusselt numbers by 0.3%, while the increase from smooth to R2 (ε/D = 0.0006) increased the friction factor by up to 9.5% and decreased the Nusselt numbers by 13%. After the test section was decommissioned and the inner surface of the tube was inspected, a considerable amount of visual deposition was found. However, when the surface was re-measured using the surface profilometer, the same surface roughness of ε/D = 0.0006 was measured.

To further investigate the deposit on the tubes surface, the duplicate tube (see Section 2.2) and the tested tube were observed under a standard optical microscope with 5× and 10× magnification, and the results are summarised in Table 4. Row A shows what the surface looked like after being sandblasted, while rows B and C show the surface after testing, where the flow direction was from the left- to the right-hand side of the page. The deposition built up in streaks, perpendicular to the flow direction. When observing row B, it is evident that some parts of the surface, such as the deepest crevices from the original roughened surface, remained free of deposition. Row C shows the tested surface after the surface roughness profile measurement was taken, and it is clear that the profilometer's detector tip dragged straight through the deposit-enhanced roughness profile, which explained the unchanged relative surface roughness measurement of 0.0006.

It can therefore be concluded that the deposit found on the inner surface of the tube may be the cause of the drastic increase in friction factors as it increased the roughness height, ε. Furthermore, it also acted as a heat resistive layer, which led to decreased Nusselt numbers. The inconsistent behaviour of R2 in comparison with smooth and R1 was deemed to be a result of the unknown composition and behaviour of the deposition under varying heat fluxes and mass flow rate conditions.

Table 4. Comparison of the duplicate tube to tested surface under microscope with 5× and 10× magnification

Surface	Magnification	
	1. 5×	2. 10×
A. Duplicate tube	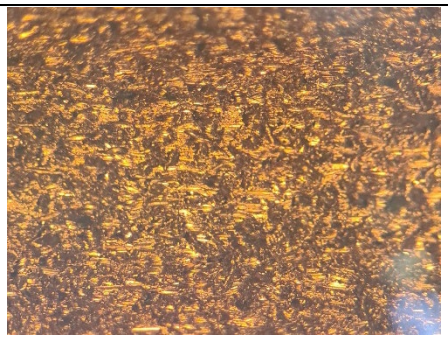	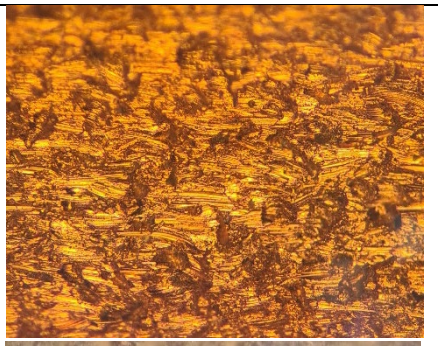
B. Tested section		
C. Tested section after surface roughness testing	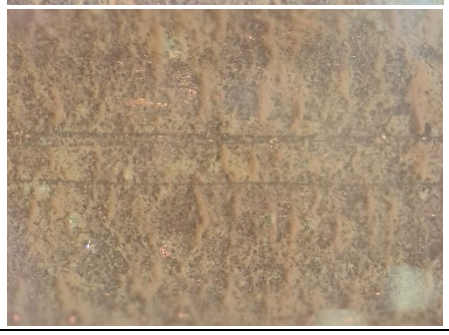	

To predict the effective relative surface roughness and effective surface roughness height of R2 with the deposition built up, the Haaland [23] friction factor equation for rough tubes (Eq. (25)) was plotted with varying ε/D values. The friction factors corresponded to $\varepsilon/D = 0.0025$, as indicated in Fig. 13, which is an order of magnitude higher than what was measured.

$$\frac{1}{\sqrt{f}} \cong -1.8 \log\left[\frac{6.9}{Re} + \left(\frac{\varepsilon/D}{3.7}\right)^{1.11}\right] \tag{25}$$

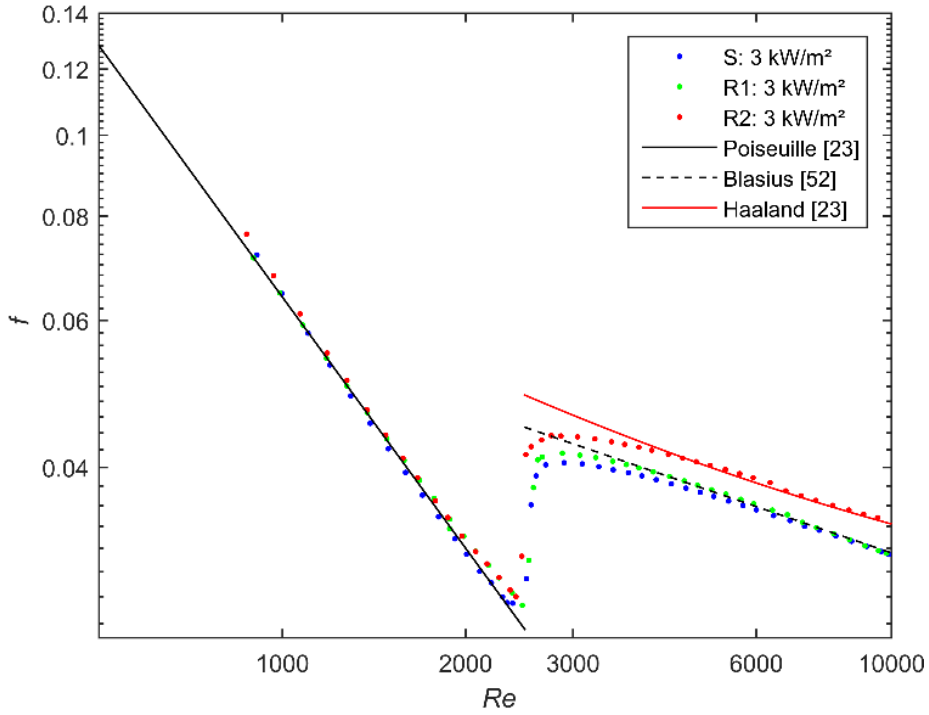

Fig. 13. Relative surface roughness prediction based on friction factor correlation of Haaland [23].

Eq. (26) was used to back-calculate the roughness height and diameter. The roughness height was subtracted from each side of the tube to account for the restricted diameter. The roughness height was calculated as 12.9 µm, compared to 3.1 µm, which was measured using the profilometer, while the diameter decreased to 5.18 µm compared to 5.20 µm. Therefore, using the equation of Haaland [23], an increase in surface roughness height of 9.55 µm was calculated which corresponds to an increase of 285%.

$$0.0025 = \frac{\varepsilon}{D - 2\varepsilon} \tag{26}$$

7.4. Flow regime boundaries and characteristics

The flow regime boundaries and transitional flow characteristics were calculated using Eqs. (20)-(22) and Eqs. (23)-(24), respectively. These equations utilised heat transfer variables, namely the Colburn *j*-factors and the Nusselt numbers to determine the start of each flow regime. Consequently, the flow regime boundaries could not be determined for the isothermal experiments using the same equations, due to the lack of heat transfer data. The flow regime boundaries for the isothermal cases were thus visually estimated. The critical Reynolds number corresponds to the point where the gradient of the Colburn *j*-factors changes from negative to positive (Eq. (20)). Because Everts and Meyer [30] found that the trends of the friction factors and Colburn *j*-factors are similar, especially in the laminar and transitional flow regimes, the same approach was used to determine the critical Reynolds number using the friction factors.

The calculated critical Reynolds numbers using the Colburn *j*-factors and friction factors are compared in Table 5. It is expected from Everts and Meyer [29], that the critical Reynolds numbers for both the heat transfer and the pressure drop coincide, as the onset of transition occurs instantaneously in the entire tube. However, the calculated critical Reynolds numbers in the smooth and R1 tubes at the 1 kW/m² and 2 kW/m² heat fluxes, did not precisely coincide.

The calculated critical Reynolds numbers based on the Colburn *j*-factors were on average 50 lower than that of the friction factors. For the friction factor data, the shift from the laminar flow regime to the transitional flow regime, near or at the critical Reynolds number was gradual whereas the shift for the Colburn *j*-factors was pronounced. This can be attributed to the fact that the pressure drop was measured across two localised points, where the surface temperatures over the same tube length were measured at 11 evenly distributed stations. Due to the sporadic nature of transition, the Colburn *j*-factors could have been more sensitive to capturing the transitional flow characteristics than the friction factors, resulting in a sharper transition for the Colburn *j*-factors. This could lead to the mischaracterisation of the critical Reynolds number in the friction factors. Additionally, the data points taken near and in the transitional flow regime were taken in intervals of approximately 50 Reynolds numbers, further contributing to the possibility of misclassifying the point of transition at lower heat fluxes and relative surface roughnesses.

When the heat flux was increased to 3 kW/m² (where the uncertainties were lower) and relative surface roughness was increased, the transition became sharper and more pronounced, therefore the criteria for the critical Reynolds number [29] was more apt and the calculated critical Reynolds numbers of the friction factors and Colburn *j*-factors coincided. It was therefore concluded that, within the uncertainties, the critical Reynolds numbers were approximately the same for both the heat transfer and pressure drop results.

Table 5: Comparison of the critical Reynolds numbers determined from the Colburn *j*-factors and friction factors.

Heat Fluxes ($\dot{q}$) [kW/m²]	**Smooth Tube**		**Rough Tube 1** $\varepsilon/D = 0.0003$		**Rough Tube 2** $\varepsilon/D = 0.0006$	
	Re_{cr} - j	Re_{cr} - f	Re_{cr} - j	Re_{cr} - f	Re_{cr} - j	Re_{cr} - f
1	1 986	2 138	2 119	2 172	2 259	2 259
2	2 222	2 268	2 254	2 300	2 386	2 386
3	2 390	2 459	2 482	2 482	2 425	2 425

To determine the influence that the surface roughness had on the flow regime boundaries and characteristics, the tests had to be compared isothermally and at the same heat fluxes and the results are summarised in Table 6 and Table 7. For isothermal flow through the smooth tube, the transitional flow regime started at a Reynolds number of 1 986, but was delayed to 2 030 for R1 and 2 174 for R2. An increase in surface roughness decreased the width of the transitional flow regime from 420 for the smooth tube to 351 and 97 for R1 and R2, respectively, while the transition gradient increased from 1.45×10^{-5} for the smooth tube to 7.16×10^{-5} for R2. For the 1 kW/m² heat flux and 2 kW/m² heat fluxes, similar trends were observed, where the onset of transition was delayed, the width of transition decreased and the gradient of transition increased when increasing the surface roughness.

However, for the 3 kW/m² heat flux, an anomaly was observed due to the deposition built-up in the tube (Section 7.3). The increase of surface roughness from smooth to R1, delayed transition from 2 390 to 2 482, however, the increase of roughness from R1 to R2, caused the start of transition to occur earlier, shifting from 2 482 to 2 425. Although the critical Reynolds number behaved in an unusual manner, the width of the transitional flow regime and the transition gradient behaved similarly to R2. The width of the transitional flow regime decreased from 172 to 86 and the transition gradient increased from 4.99×10^{-5} to 14.6×10^{-5} when increasing the relative surface roughness from $\varepsilon/D \approx 0$ to $\varepsilon/D = 0.0006$.

Table 6: Flow regime boundaries

Heat Fluxes ($\dot{q}$) **[kW/m²]**	**Smooth Tube**			**Rough Tube 1** ε/D **= 0.0003**			**Rough Tube 2** ε/D **= 0.0006**		
	Re_{cr}	Re_{qt}	Re_t	Re_{cr}	Re_{qt}	Re_t	Re_{cr}	Re_q	Re_t
0	1 985	2 408	8 014	2 030	2 381	7 965	2 174	2 271	7 912
1	1 986	2 440	8 048	2 119	2 462	7 961	2 259	2 357	7 947
2	2 222	2 518	8 080	2 254	2 447	8 007	2 386	2 484	7 975
3	2 390	2 562	8 099	2 482	2 628	8 044	2 425	2 511	8 010

Table 7: Transitional flow metrics.

Heat Fluxes ($\dot{q}$) **[kW/m²]**	**Smooth Tube**		**Rough Tube 1** ε/D **= 0.0003**		**Rough Tube 2** ε/D **= 0.0006**	
	ΔRe	TG_j	ΔRe	TG_j	ΔRe	TG_j
0	420	1.45×10^{-5}	351	1.73×10^{-5}	97	7.16×10^{-5}
1	454	1.25×10^{-5}	343	2.40×10^{-5}	98	7.70×10^{-5}
2	296	3.29×10^{-5}	193	3.81×10^{-5}	98	13.4×10^{-5}
3	172	4.99×10^{-5}	146	9.01×10^{-5}	86	14.6×10^{-5}

Everts and Meyer [29] concluded that, for smooth tubes, an increase in heat flux delayed the onset of transition, decreased the width of the transitional flow regime and increased the transition gradient. For the smooth tube, Table 6 indicates that the critical Reynolds number increased from 1 986 at a heat flux of 1 kW/m^2 to 2 222 and 2 390 at heat fluxes of 2 kW/m^2 and 3 kW/m^2, respectively. Furthermore Table 7 indicates that the width of the transitional flow regime decreased from 454 to 172, and the transition gradient increased from 1.25×10^{-5} to 4.99×10^{-5} when increasing the heat flux from 1 kW/m^2 to 3 kW/m^2. Similar trends were also observed in the two rough tubes. However, Table 7 indicates that the effect of heat flux decreased with increasing surface roughness. This is due to the flow disturbances created by the surface roughness profile that dampened and disturbed secondary flow effects.

The end of the transitional flow regime, which corresponds to the start of the quasi-turbulent flow regime, occurred at lower Reynolds numbers as the surface roughness was increased. This contributed to the decreasing width of the transitional flow regime and increasing transition gradients with increasing surface roughness. Furthermore, an increase in heat flux from 1 kW/m^2 to 3 kW/m^2 also delayed the onset of the quasi-turbulent flow regime from 2 440 to 2 562 in the smooth tube and similar trends were again observed in the two rough tubes.

Similar to the quasi-turbulent flow regime, an increase in surface roughness caused the turbulent flow regime to start at lower Reynolds numbers. Although the Reynolds numbers decreased, it was noted that the onset of the turbulent flow regime occurred at approximately the same mass flow rates for smooth, R1 and R2 at each heat flux. Under isothermal conditions, Re_t occurred at a mass flow rate of 0.0325 kg/s. For the 1 kW/m^2 heat flux, it occurred at a mass flow rate of 0.0322 kg/s, while for 2 kW/m^2 and 3 kW/m^2, Re_t occurred at 0.0319 kg/s and 0.0316 kg/s, respectively. The differing Reynolds numbers were therefore due to the differing fluid properties with temperature. Furthermore, the changes in fluid properties with

temperature also caused a slight delay in the start of the turbulent flow regime with the increasing of heat fluxes from 8 014 for the isothermal case to 8 048 for 1 kW/m^2, 8 080 for 2 kW/m^2 and 8 099 for 3 kW/m^2. This behaviour shows that rough tubes behave in a similar manner to smooth tubes on a macro-scale when heat flux was increased.

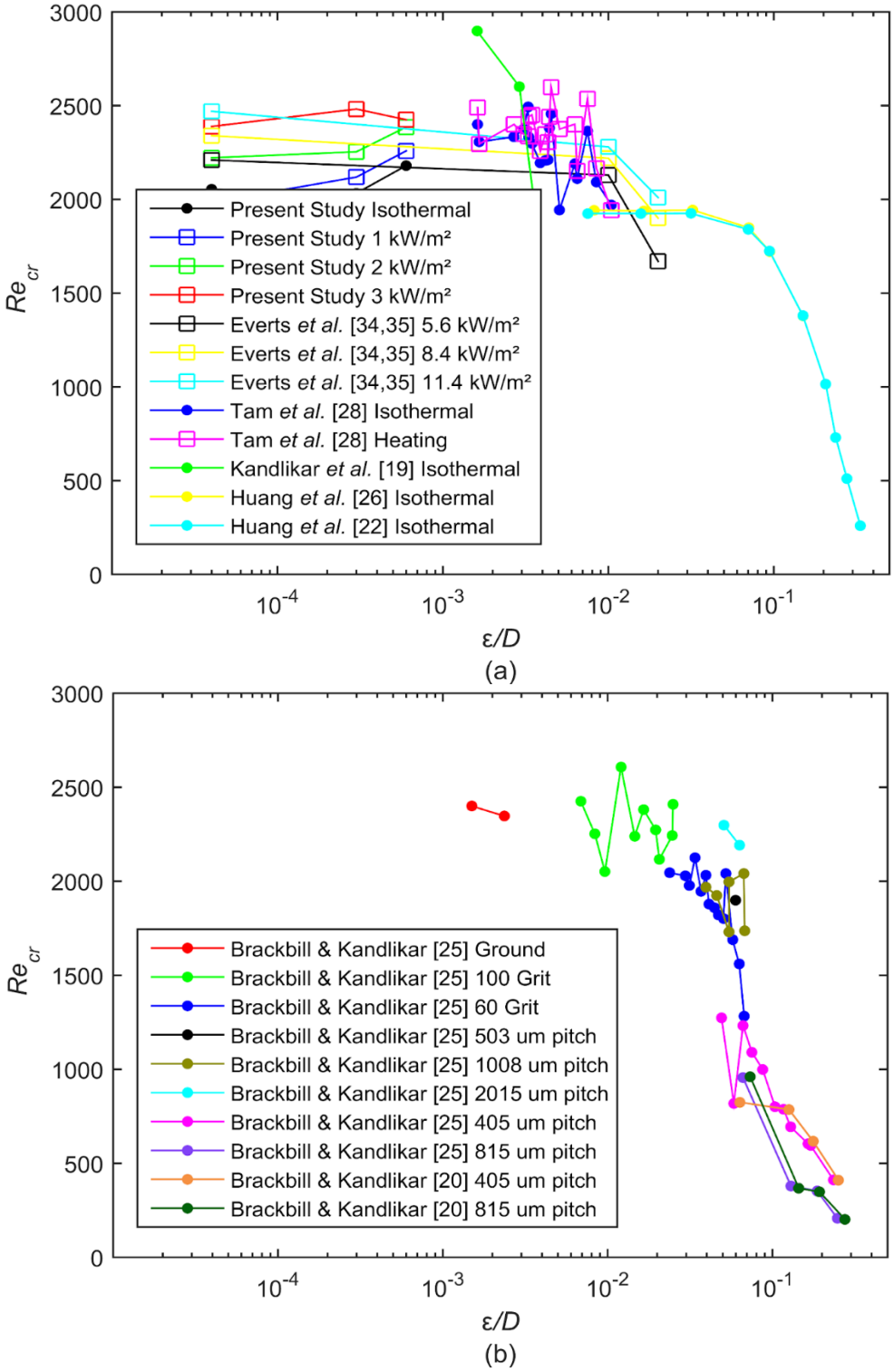

Fig. 14: The critical Reynolds number, Re_{cr}, behaviour as a function of relative surface roughness, ε/D, using (a) the base diameter and (b) the constricted flow diameter.

An unexpected trend found in this study was that an increase in surface roughness generally delayed the onset of transition, which is contradictory when compared to the findings of other authors [15, 19-21, 25, 27, 28]. The findings of other authors' critical Reynolds numbers with varying relative surface roughness are summarised in Fig. 14. Fig. 14(a) compares the critical Reynolds numbers of studies that used the base diameter, while Fig. 14(b) compares the critical Reynolds numbers as a function of relative surface roughness calculated using the constricted flow diameter. In Fig. 14(a), the isothermal and diabatic results are represented by circle and square markers, respectively, while Fig. 14(b) contains isothermal results only.

From Fig. 14(a) it follows that the surface roughness values tested in this study were the lowest compared to previous studies investigating the influence of surface roughness on the critical Reynolds numbers. The critical Reynolds numbers increased with increasing surface roughness. An increase in heat flux also caused a delay in transition, however, the effect became less as the surface roughness was increased. Tam *et al.* [28] used mini-tubes with surface roughnesses of approximately an order of magnitude greater than in this study. The isothermal results showed a decrease in the critical Reynolds number with increasing surface roughness. Although some scatter existed in their diabatic results, it seems as if the critical Reynolds numbers remained approximately constant up to $\varepsilon/D = 0.005$ and then it began to decrease as the Reynolds number was increased. The macro-tube results of Everts *et al*. [34, 35] and Huang *et al*. [22, 26] were in the order of 0.01-1 and showed a significant decrease in the critical Reynolds number with increasing surface roughness.

From Fig. 14(b) it follows that similar trends were observed in the study of Brackbill and Kandlikar [25] who made used of the constricted flow diameter. For relative surface roughness values between 0.0015 and 0.025, the critical Reynolds number decreased gradually with increasing surface roughness, while a significant decrease in critical Reynolds number was observed for relative surface roughness values greater than 0.025.

From the results of this study, as well as those of previous studies, summarised in Fig. 14, it was proposed that the general trend that occurs in the critical Reynolds numbers due to the increase in the surface roughness and heat flux, can be represented schematically by Fig. 15. In Fig. 15, the increase in the heat flux (and thus an increase in the modified Grashof number) is indicated schematically by the line colours (black to red). The "scatter" in the data from Fig. 14 was omitted to clarify the trends and highlights the areas where more research needs to be conducted to improve our current understanding. Three distinct regions can be identified: (1) Dampening region ($\varepsilon/D \leq \varepsilon_1/D$), (2) Enhancing ($\varepsilon_1/D \leq \varepsilon/D \leq \varepsilon_2/D$) and (3) Saturating region ($\varepsilon/D \geq \varepsilon_2/D$), where ε_1 and ε_2 are proposed to be in the order of 0.001 and 0.01, respectively.

In the Dampening region, the relative surface roughnesses are low, such as the surface roughnesses attained in this study, and the general trend is that the critical Reynolds number increases with increasing surface roughness. Previous studies conducted using smooth tubes [39-42] found that transition is delayed for smoother inlet geometries. A square-edged inlet is commonly used in experimental studies, as well as practical applications, and this inlet is characterised by a sudden contraction from the flow-calming section diameter (or header of the heat exchanger) to the test section. When compared to a smooth tube, the low surface roughness slightly disturbs the flow when entering the tube. However, this disturbance is so small, that the effect is to rather smoothen the inlet, thus dampening the inlet disturbances and delays the start of the transitional flow regime. As the relative surface roughness in this region is very low, the associated flow disturbances are not sufficient to dominate secondary flow effects, and therefore an increase in heat flux (and thus modified Grashof number) has a significant effect, namely to increase the critical Reynolds numbers.

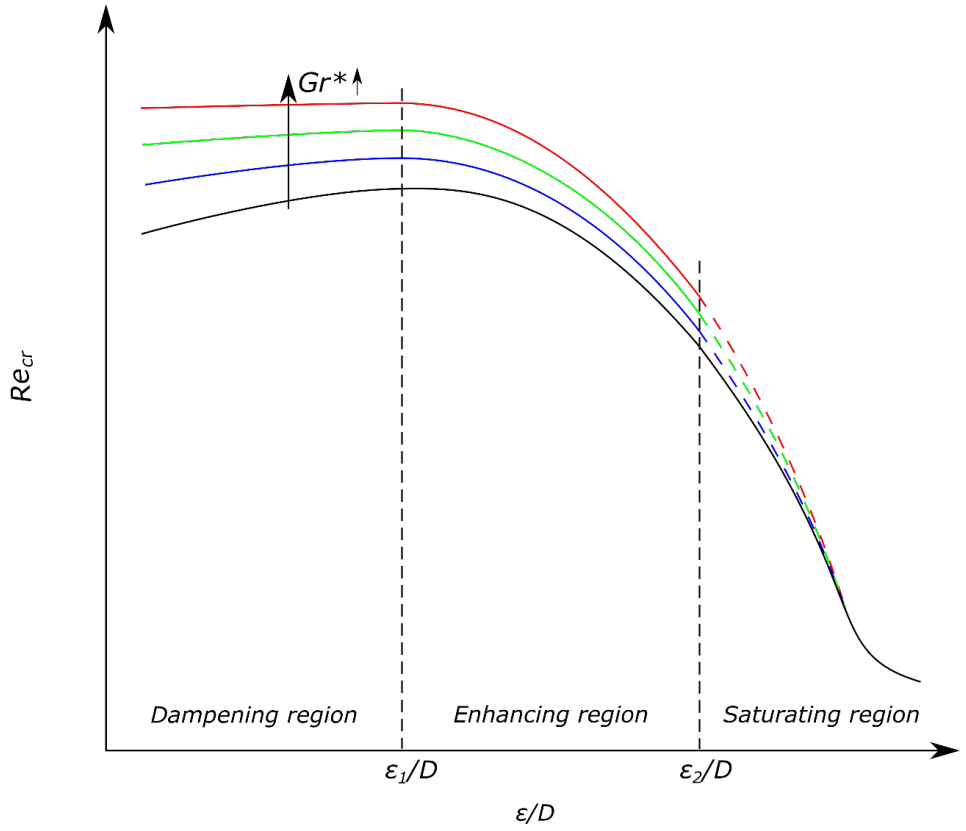

Fig. 15: Schematic summary of the influence of surface roughness on the critical Reynolds number, Re_{cr}, indicating the (1) Dampening region ($\varepsilon/D \leq \varepsilon_1/D$), (2) Enhancing ($\varepsilon_1/D \leq \varepsilon/D \leq \varepsilon_2/D$) and (3) Saturating region ($\varepsilon/D \geq \varepsilon_2/D$).

The Enhancing region ($\varepsilon_1/D \leq \varepsilon/D \leq \varepsilon_2/D$) represents moderate relative surface roughnesses and the general trend is that the critical Reynolds number decreases with increasing surface roughness. The flow disturbances created by the roughness elements disturbs the flow in the boundary layer and are sufficient to initiate the flow and temperature fluctuations that are associated with transitional flow. These flow disturbances suppress secondary flow effects, and therefore the influence of modified Grashof number is less in this region and decreases further with increasing surface roughness.

In the Saturating region ($\varepsilon/D \geq \varepsilon_2/D$), the relative surface roughnesses becomes significantly large up to the point where the tube almost resembles that of a porous tube. The flow disturbances caused by these roughness elements are severe enough to cause flow fluctuations inside the tube and the flow transitions from laminar to turbulent, without a noteworthy transition region. A similar trend was observed by Everts and Meyer [29], where mixed convection effects enhanced the transitional flow fluctuations to such an extent that the flow transitioned from pure laminar flow at one Reynolds number to quasi-turbulent flow at the next Reynolds number, skipping the entire transitional flow regime. As these roughness elements are very significant in comparison to the diameter, the shapes of the roughness elements may have a more significant effect on the critical Reynolds number rather than the mean height of the roughness elements. This means that vastly different relative surface roughnesses, above, ε_2/D, could result in similar critical Reynolds numbers. The Grashof number is expected to have a negligible effect in this region, as all secondary flow effects would be suppressed by the flow disturbances inside the rough tube. However, more experiments at different Grashof

numbers need to be conducted to gain a complete understanding of the influence of surface roughness in this region.

7.5. Simultaneous heat transfer and pressure drop

Throughout previous studies, it has been difficult for authors to simultaneously measure heat transfer and pressure drop within macro-scale rough tubes that mimic natural roughness. This was due to the process of producing a roughness profile on the inner surface of the tube, which typically resulted in an alteration of the test section's physical properties, hindering accurate heat transfer measurements. Due to the surface roughness in the present study being produced through a sand blasting process, simultaneous heat transfer and pressure drop measurements were possible as the physical properties of the test section remained unaltered. Increasing the surface roughness was hypothesised to improve heat transfer by increasing mixing in the boundary layers and consequently increase the pressure drop through the test section.

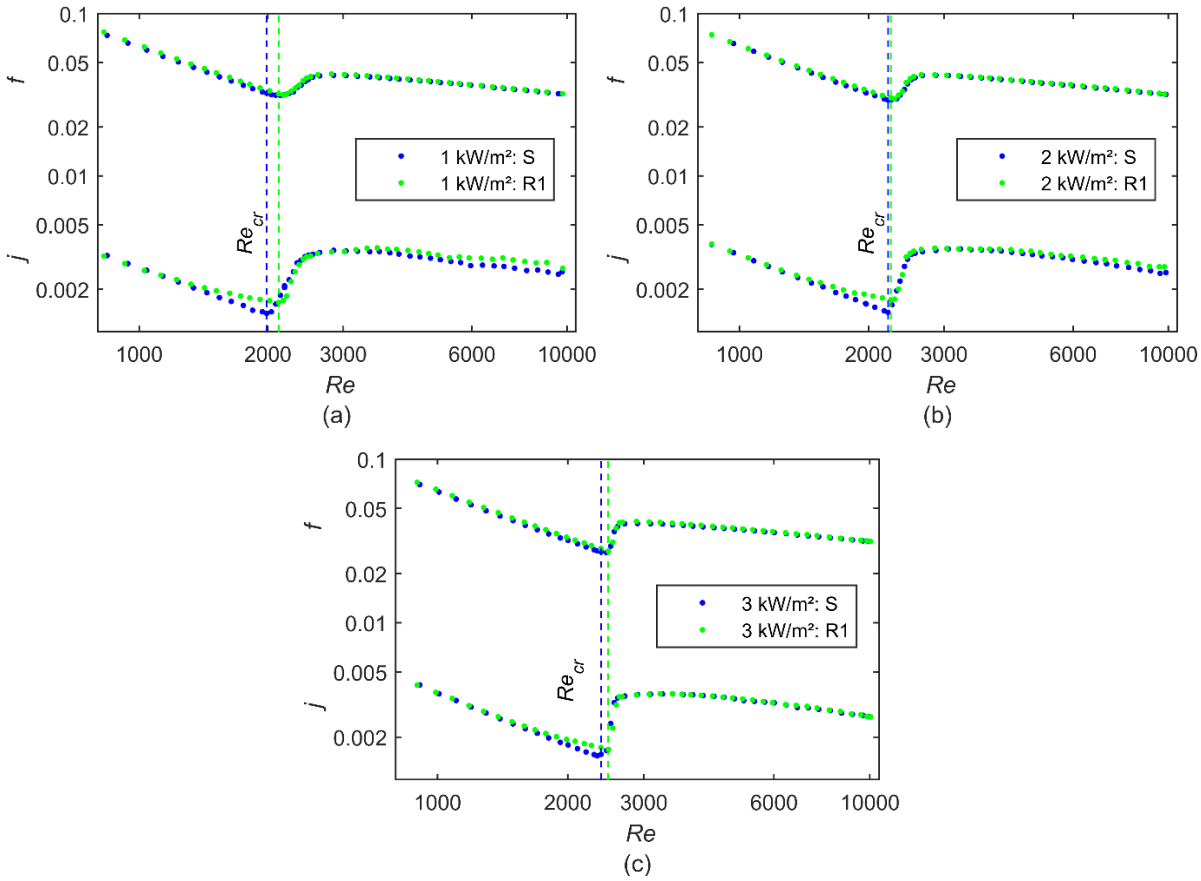

Fig. 16: Simultaneous comparison of the Colburn *j*-factors and friction factors as a function of Reynolds number at two relative surface roughnesses for the heat fluxes of (a) 1 kW/m², (b) 2 kW/m² and (c) 3 kW/m².

The Colburn *j*-factors and the friction factors were simultaneously plotted with respect to the Reynolds number for each heat flux in Fig. 16(a-c) to compare the effects of the surface roughness on the heat transfer coefficients and the friction factors. Due to the discrepancies found in R2 (as a result of deposition on the tube surface), they have been omitted in this graph. As expected from previous studies which were performed using smooth tubes, such as Everts and Meyer [30], it follows from Fig. 16 that the trends of the Colburn *j*-factors and friction factors were similar in all flow regimes.

In general, it was concluded the boundaries between the flow regimes were the same for heat transfer and pressure drop. Therefore, the friction factors were divided by the Colburn *j*-factors (*f*/*j*-factor) and plotted in Fig. 17 to investigate the effects of the surface roughness on the relationship between the heat transfer and pressure drop. The *f*/*j*-factor is useful, as it represents the reciprocal of the performance of the test section. A lower *f*/*j*-factor is more desirable as this represents an increase in heat transfer whilst minimizing pressure drop.

For the smooth tube, the laminar *f*/*j*-factors increased as the Reynolds number increased for each heat flux. Furthermore, the magnitude of the laminar *f*/*j*-factors decreased with increasing heat flux, while the gradient increased. R1 followed a similar trend at lower laminar Reynolds numbers. However, at higher laminar Reynolds numbers, the *f*/*j*-factors decreased below that of the smooth tube. This indicated the surface roughness had a greater and favourable effect on the heat transfer coefficients than on the friction factors.

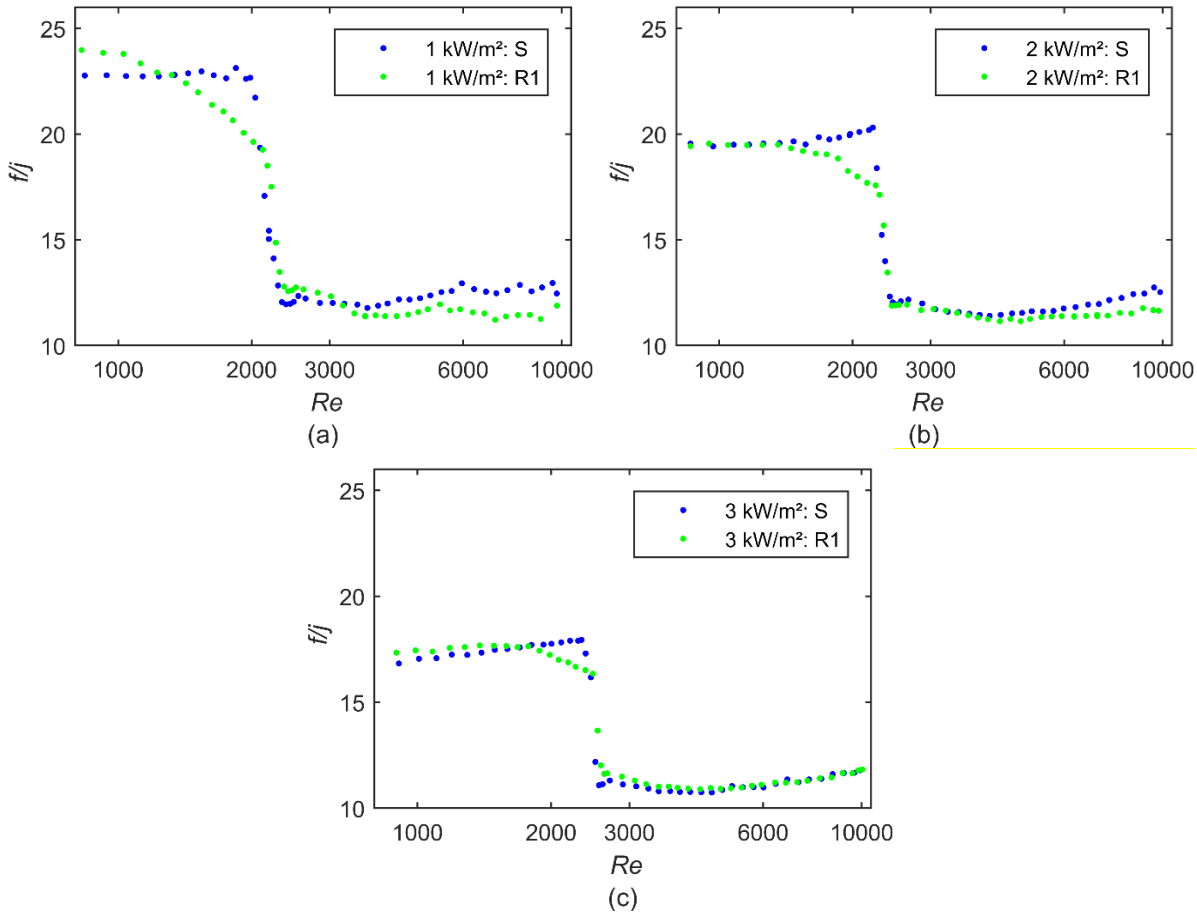

Fig. 17: Comparison of the *f*/*j*-factors with respect to the Reynolds numbers for two relative surface roughnesses at heat fluxes of (a) 1 kW/m², (b) 2 kW/m² and (c) 3 kW/m².

This change in trend occurred at a Reynolds number of approximately 1 028, when a heat flux of 1 kW/m² was applied, but was delayed to Reynolds numbers of approximately 1 358 and 1 778 when the heat flux was increased to 2 kW/m² and 3 kW/m², respectively. When comparing these Reynolds numbers to the results in Fig. 16, as well as in Sections 7.1 and 7.2, it follows that these Reynolds numbers corresponded to the Reynolds numbers at which the heat transfer coefficients and friction factors began to deviate from the expected fully developed trends. The general trend in Fig. 16, however, shows that the surface roughness had a larger influence on the heat transfer than on the pressure drop. At a heat flux of 1 kW/m² (Fig. 16(a)) and Reynolds number of approximately 1 900, a maximum increase of 19% and

6% was found in the Colburn *j*-factors and friction factors, respectively. This was similar to the 2 kW/m² heat flux (Fig. 16(b)) at a Reynolds number of 2 150, where the increases were 20% and 5% for the Colburn *j*-factors and friction factors, respectively. A smaller change was observed for the 3 kW/m² heat flux (Fig. 16(c)), where at a Reynolds number of approximately 2 300, the Coburn *j*-factors increased by only 13% and the friction factors increased by 6%. It can therefore be postulated that rough tubes are more favourable for developing flow conditions than fully developed flow.

The *f*/*j*-factors decreased significantly with increasing Reynolds number in the transitional flow regime. Although the transitional flow regime was found to be delayed and shorter for rough tubes than for smooth tubes (Section 7.4), there was a negligible difference between the gradient of *f*/*j*-factors of the smooth and rough tubes. At a specific Reynolds number, the *f*/*j*-factors of the rough tube were slightly higher than that of the smooth tube. A possible reason for this is that the temperature, mass flow rate and pressure drop fluctuations that occurred in the transitional flow regime [29, 30] were enhanced by the surface roughness, which led to a greater increase in friction factors than for the smooth tubes.

At lower Reynolds numbers in the quasi-turbulent flow regime, the *f*/*j*-factors in the smooth tube were slightly lower than that of R1. As the Reynolds number increased towards the turbulent flow regime, the difference between smooth and R1 became negligible. This suggests that, in the quasi-turbulent and turbulent flow regimes, the smooth tube performed better than R1 at lower Reynolds numbers, but thereafter the performance was similar. At the 1 kW/m² and 2 kW/m² heat fluxes (Fig. 17(a) and (b)), it was generally observed that R1 produced lower *f*/*j*-factors than the smooth tube in the quasi-turbulent and turbulent flow regimes. Due to the higher uncertainties of the heat transfer coefficients at these heat fluxes, it may be misguided to conclude that these low relative surface roughnesses improved performance in the quasi-turbulent and turbulent flow regimes.

8. Conclusions

Limited previous experiments have investigated the influence of surface roughness in the transitional flow regime, however, the experiments either altered the physical properties of the tube, hindering the ability to accurately measure heat transfer, or solely measured pressure drop. Therefore, an experimental investigation of the influence of surface roughness on simultaneous heat transfer and pressure drop in the transitional flow regime was performed, focussing on three macro-scale tubes with low relative surface roughness values of $\varepsilon/D \approx 0$ (smooth), $\varepsilon/D = 0.0003$ and $\varepsilon/D = 0.0006$. The test section had an inside diameter of 5.14 mm and a length of 5.45 m, which was sufficiently long to investigate fully developed flow. The experiments were performed over a Reynolds number range which covered all four flow regimes, ensuring that the full influence of the surface roughness on heat transfer and pressure drop could be investigated. A flow-calming section with a square-edged inlet was used and the experiments were performed at heat fluxes of 0, 1, 2 and 3 kW/m^2.

It was found that the increase in surface roughness delayed the onset of the transitional flow regime, decreased the width of the transitional flow regime and increased the transition gradient, for both isothermal and diabatic conditions. An increase in heat flux further delayed the onset of the transitional flow regime, decreased the width of the transitional flow regime and increased the transition gradient, however, the effect decreased as the surface roughness was increased.

The delay of the onset of the transitional flow regime with increasing surface for low relative surface roughness values initially contradicted the previous findings obtained using tubes with moderate to high values of relative surface roughness. After combining the results of this study

with those of previous studies, an improved understanding of the influence of surface roughness on the critical Reynolds number was obtained. However, to obtain a complete understanding of the influence of surface roughness on the critical Reynolds number, more experiments need to be conducted in macro-tubes with moderate to high values of relative surface roughness at different Grashof numbers.

When investigating the influence of surface roughness on the critical Reynolds number, three distinct regions were identified and defined as the Dampening region, Enhancing region and Saturating region. In the Dampening region, the relative surface roughnesses are low, such as the surface roughnesses attained in this study, and the general trend is that the critical Reynolds number increases with increasing surface roughness. Furthermore, the associated flow disturbances are not sufficient to dominate secondary flow effects, and therefore an increase in Grashof number has a significant effect, namely to increase the critical Reynolds numbers. The Enhancing region represents moderate relative surface roughnesses and the general trend is that the critical Reynolds number decreases with increasing surface roughness. As the flow disturbances are sufficient to suppress secondary flow effects, the influence of Grashof number is less in this region and decreases further with increasing surface roughness. In the Saturating region, the flow disturbances caused by these roughness elements are severe enough to cause flow fluctuations inside the tube and the flow transitions from laminar to turbulent, without a noteworthy transition region.

From the simultaneous heat transfer and pressure drop analysis, it was found that the friction factors and the Colburn j-factors followed similar trends throughout the tested Reynolds range and the transitional flow regime occurred at approximately the same Reynolds numbers. To investigate the suitability of rough tubes, f/j-factors were calculated for all flow regimes. A lower f/j-factor is more desirable as this represents an increase in heat transfer whilst minimizing pressure drop. In the laminar flow regime, near the critical Reynolds number, it was found that the increase in surface roughness generally increased the Colburn j-factors by a factor of two more than the corresponding increase in friction factors. Furthermore, it was found that rough tubes were more favourable for developing flow, than for fully developed flow. The f/j-factors indicated that an increase in surface roughness is not favourable in the transitional flow regime as the flow disturbances further increase the transitional flow fluctuations. It was also concluded that the smooth tube generally performed better than the rough tube in the quasi-turbulent and turbulent flow regimes.

Credit authorship contribution statement

Marilize Everts: conceptualization, resources, methodology, data curation, formal analysis, investigation, validation, project administration, funding acquisition, writing: review and editing to final paper, supervision (senior lecturer).

Pascal Robbertse: methodology, validation, experiments (heat transfer), investigation, writing original draft to final paper (master's degree student).

Blayne Spitholt: methodology, validation, experiments (pressure drop), investigation, writing original draft to final paper (master's degree student).

Declaration of Competing Interest

The authors declared that there is no conflict of interest.

Acknowledgements
The funding obtained in South Africa from the Department of Science and Innovation (DSI), and University of Pretoria is acknowledged and duly appreciated.

References

[1] A. Garcia, J.P. Solano, A. Viedma, P.G. Vicente, The influence of artificial roughness shape on heat transfer enhancement: Corrugated tubes, dimpled tubes and wire coils, Applied Thermal Engineering, 35(1) (2012) 196-201.
[2] H.K. Tam, L.M. Tam, A.J. Ghajar, S.C. Tam, T. Zhang, Experimental investigation of heat transfer, friction factor, and optimal fin geometries for the internally microfin tubes in the transition and turbulent regions, Journal of Enhanced Heat Transfer, 19(5) (2012) 457-476.
[3] J.P. Meyer, S.M. Abolarin, Heat transfer and pressure drop in the transitional flow regime for a smooth circular tube with twisted tape inserts and a square-edged inlet, International Journal of Heat and Mass Transfer, 117 (2018) 11-29.
[4] J.P. Meyer, J.A. Olivier, Transitional flow inside enhanced tubes for fully developed and developing flow with different types of inlet disturbances: Part I - Adiabatic pressure drops, International Journal of Heat and Mass Transfer, 54(7-8) (2011) 1587-1597.
[5] J.P. Meyer, J.A. Olivier, Transitional flow inside enhanced tubes for fully developed and developing flow with different types of inlet disturbances: Part II-heat transfer, International Journal of Heat and Mass Transfer, 54(7-8) (2011) 1598-1607.
[6] Z.S. Kareem, M.N. Mohd Jaafar, T.M. Lazim, S. Abdullah, A.F. Abdulwahid, Passive heat transfer enhancement review in corrugation, Experimental Thermal and Fluid Science, 68 (2015) 22-38.
[7] W. Cope, The friction and heat transmission coefficients of rough pipes, Proceedings of the Institution of Mechanical Engineers, 145(1) (1941) 99-105.
[8] D.F. Dipprey, R.H. Sabersky, Heat and momentum transfer in smooth and rough tubes at various prandtl numbers, International Journal of Heat and Mass Transfer, 6(5) (1963) 333-332.
[9] J. Nikuradse, Laws of Flow in Rough Pipes, National Advisory Committee for Aeronautics Washington, 1933.
[10] H. Darcy, Recherches Expérimentales Eelatives au Mouvement de L'Eau dans les Tuyaux, Mallet-Bachelier, Paris, 1857.
[11] J.T. Fanning, A Practical Treatise on Hydraulic and Water Supply Engineering, Van Nostrand, New York, 1882.
[12] S.G. Kandlikar, D. Schmitt, A.L. Carrano, J.B. Taylor, Characterization of surface roughness effects on pressure drop in single-phase flow in minichannels, Physics of Fluids, 17(10) (2005) 100606.
[13] C.F. Colebrook, Turbulent flow in pipes, with particular reference to the transition region between the smooth and rough pipe laws, Journal of the Institution of Civil Engineers, 11(4) (1939) 133-156.
[14] L.F. Moody, Friction factors for pipe flow, Trans. ASME, 66 (1944) 671-684.
[15] S. Kandlikar, Roughness effects at microscale - reassessing Nikuradse's experiments on liquid flow in rough tubes, Bulletin of the Polish Academy of Sciences: Technical Sciences, 53(4) (2005).
[16] R.L. Webb, E.R.G. Eckert, R.J. Goldstein, Heat transfer and friction in tubes with repeated-rib roughness, International Journal of Heat and Mass Transfer, 14(4) (1971) 601-617.
[17] T. Adams, C. Grant, H. Watson, A simple algorithm to relate measured surface roughness to equivalent sand-grain roughness, International Journal of Mechanical Engineering and Mechatronics, 1(2) (2012) 66-71.
[18] F.F. Farshad, H.H. Rieke, Surface-roughness design values for modern pipes, SPE Drilling & Completion, 21(3) (2006) 212-215.
[19] S.G. Kandlikar, S. Joshi, S. Tian, Effect of surface roughness on heat transfer and fluid flow characteristics at low reynolds numbers in small diameter tubes, Heat Transfer Engineering, 24(3) (2003) 4-16.
[20] T. Brackbill, S. Kandlikar, Effects of low uniform relative roughness on single-phase friction factors in microchannels and minichannels, in: ASME 5th International Conference on Nanochannels, Microchannels, and Minichannels, ASME, Puebla, Mexico, 2007, pp. 509-518.
[21] A.J. Ghajar, C.C. Tang, W.L. Cook, Experimental investigation of friction factor in the transition region for water flow in minitubes and microtubes, Heat Transfer Engineering, 31(8) (2010) 646-657.

[22] K. Huang, J.W. Wan, C.X. Chen, Y.Q. Li, D.F. Mao, M.Y. Zhang, Experimental investigation on friction factor in pipes with large roughness, Experimental Thermal and Fluid Science, 50 (2013) 147-153.
[23] Y.A. Çengel, A.J. Ghajar, Heat and mass transfer : fundamentals & applications, Fifth edition in SI units. ed., Mcgraw Hill Education, New York, 2015.
[24] Z.-X. Li, D. Du, Z.-Y. Guo, Experimental study on flow characteristics of liquid in circular microtubes, Microscale Thermophysical Engineering, 7 (2003) 253-265.
[25] T.P. Brackbill, S.G. Kandlikar, Application of lubrication theory and study of roughness pitch during laminar, transition, and low reynolds number turbulent flow at microscale, Heat Transfer Engineering, 31(8) (2010) 635-645.
[26] K. Huang, J.W. Wan, C.X. Chen, D.F. Mao, Y.Q. Li, Experiments investigation of the effects of surface roughness on laminar flow in macro tubes, Experimental Thermal and Fluid Science, 45 (2013) 243-248.
[27] D. Schmitt, S. Kandlikar, Effects of repeating microstructures on pressure drop in rectangular minichannels, in: ASME 3rd International Conference on Microchannels and Minichannels, ASME, Toronto, Ontario, Canada, 2005, pp. 281-289.
[28] L.M. Tam, H.K. Tam, A.J. Ghajar, N. Wa San, C.K. Wu, The effect of inner surface roughness and heating on friction factor in horizintal mini-tubes., in: 15th International Heat Transfer Conference, Kyoto, Japan, 2014, pp. 1-13.
[29] M. Everts, J.P. Meyer, Heat transfer of developing and fully developed flow in smooth horizontal tubes in the transitional flow regime, International Journal of Heat and Mass Transfer, 117(5) (2018) 1331-1351.
[30] M. Everts, J.P. Meyer, Relationship between pressure drop and heat transfer of developing and fully developed flow in smooth horizontal circular tubes in the laminar, transitional, quasi-turbulent and turbulent flow regimes, International Journal of Heat and Mass Transfer, 117(8) (2018) 1231-1250.
[31] I.E. Idelchik, Handbook of Hydraulic Resistance, Israel Program For Scientific Translations, Washington, 1986.
[32] G.P. Celata, M. Cumo, M. Guglielmi, G. Zummo, Experimental investigation of hydraulic and single-phase heat transfer In 0.130-mm capillary tube, Microscale Thermophysical Engineering, 6(2) (2002) 85-97.
[33] Y. Zhao, Z. Liu, Experimental studies on flow visualization and heat transfer characteristics in microtubes, in: 13th International Heat Transfer Conference, Begell House Inc., Sydney, Australia, 2006, pp. 12-12.
[34] M. Everts, S. Ayres, F. Houwer, C. Vanderwagen, N. Kotze, J. Meyer, The influence of surface roughness on heat transfer in the transitional flow regime, in: 15th International Heat Transfer Conference, Kyoto, Japan, 2014, pp. 1-12.
[35] J. Meyer, M. Everts, S.R. Ayres, F.A. Mulock-Houwer, C.P. Vanderwagen, N. Kotze, The influence of surface roughness in the transitional flow regime of a parabolic trough receiver tube, in: 2nd Southern African Energy Conference, Port Elizabeth, South Africa, 2014.
[36] J. Meyer, Heat transfer in tubes in the transitional flow regime, in: 15th International Heat Transfer Conference, Kyoto, Japan, 2014, pp. 1-12.
[37] P.L. Young, T.P. Brackbill, S.G. Kandlikar, Comparison of roughness parameters for various microchannel surfaces in single-phase flow applications, Heat Transfer Engineering, 30(1-2) (2009) 78-90.
[38] M. Everts, Heat transfer and pressure drop of developing flow in smooth tubes in the transitional flow regime, Master's Thesis, University of Pretoria, 2014.
[39] A.J. Ghajar, K.F. Madon, Pressure drop measurements in the transition region for a circular tube with three different inlet configurations, Experimental Thermal and Fluid Science, 5(1) (1992) 129-135.
[40] A.J. Ghajar, L.-M. Tam, Heat transfer measurements and correlations in the transition region for a circular tube with three different inlet configurations, Experimental Thermal and Fluid Science, 8(1) (1994) 79-90.

[41] L.-M. Tam, A.J. Ghajar, Effect of inlet geometry and heating on the fully developed friction factor in the transition region of a horizontal tube, Experimental Thermal and Fluid Science, 15(1) (1997) 52-64.
[42] H.K. Tam, L.M. Tam, A.J. Ghajar, Effect of inlet geometries and heating on the entrance and fully-developed friction factors in the laminar and transition regions of a horizontal tube, Experimental Thermal and Fluid Science, 44 (2013) 680-696.
[43] J.P. Meyer, M. Everts, Single-phase mixed convection of developing and fully developed flow in smooth horizontal circular tubes in the laminar and transitional flow regimes, International Journal of Heat and Mass Transfer, 117 (2018) 1251-1273.
[44] M. Everts, J.P. Meyer, Flow regime maps for smooth horizontal tubes at a constant heat flux, International Journal of Heat and Mass Transfer, 117 (2018) 1274-1290.
[45] R. Rayle, Influence of orifice geometry on static pressure measurements, American Society of Mechanical Engineers, No. 59-A-234 (1959).
[46] R.E. Rayle, An investigation of the influence of orifice geometry on static pressure measurements, Master's Thesis, Massachusetts Institute of Technology, 1949.
[47] M. Everts, J.P. Meyer, Laminar hydrodynamic and thermal entrance lengths for simultaneously hydrodynamically and thermally developing forced and mixed convective flows in horizontal tubes, Experimental Thermal and Fluid Science, 118 (2020).
[48] C.O. Popiel, J. Wojtkowiak, Simple formulas for thermophysical properties of liquid water for heat transfer calculations (from 0°C to 150°C), Heat Transfer Engineering, 19(3) (1998) 87-101.
[49] P.F. Dunn, Measurement and Data Analysis for Engineering and Science, 2nd ed., CRC Press/Taylor & Francis, Boca Raton, FL, 2010.
[50] M. Everts, Single-phase mixed convection of developing and fully developed flow in smooth horizontal tubes in the laminar, transitional, quasi-turbulent and turbulent flow regimes, University of Pretoria, Pretoria, 2017.
[51] J.P. Meyer, M. De Paepe, Test Sections for Heat Transfer and Pressure Drop Measurements: Construction, Calibration, and Validation, in: The Art of Measuring in the Thermal Sciences, CRC Press, 2020, pp. 107-158.
[52] F.M. White, Fluid Mechanics, 7th (SI units) ed., McGraw-Hill, Singapore, 2011.
[53] R.K. Shah, A.L. London, Laminar Flow Forced Convection in Ducts, Academic Press, New York, 1978.
[54] S.M. Morcos, A.E. Bergles, Experimental investigation of combined forced and free laminar convection in horizontal tubes, Journal of Heat Transfer, 97(2) (1975) 212-219.
[55] J.P. Meyer, M. Everts, N. Coetzee, K. Grote, M. Steyn, Heat transfer coefficients of laminar, transitional, quasi-turbulent and turbulent flow in circular tubes, International Communications in Heat and Mass Transfer, 105 (2019) 84-106.
[56] V. Gnielinski, Corrigendum to “On heat transfer in tubes” [International Journal of Heat and Mass Transfer 63 (2013) 134–140], International Journal of Heat and Mass Transfer, 100(81) (2015) 638.
[57] H. Blasius, Das Ähnlichkeitsgesetz bei Reibungsvorgängen in Flüssigkeiten, in: Mitteilungen über Forschungsarbeiten auf dem Gebiete des Ingenieurwesens (insbesondere der Technischen Hochschulen), Springer, Berlin, 1913, pp. 1-41.